JCI insight

Recurrent moderate hypoglycemia accelerates the progression of cognitive deficits through impairment of TRPC6/GLUT3 pathway in diabetic APP/PS1 mice

Chengkang He, … , Martin Tepel, Zhiming Zhu

JCI Insight. 2022. https://doi.org/10.1172/jci.insight.154595.

Research In-Press Preview **Endocrinology**

Currently, the most effective strategy for dealing with Alzheimer's disease (AD) is delaying the onset of dementia. Severe hypoglycemia is strongly associated with dementia; however, the effects of recurrent moderate hypoglycemia (RH) on progression of cognitive deficits in diabetic patients with genetic susceptibility to AD remain unclear. Here, we report that insulin-controlled hyperglycemia only slightly aggravated AD-type pathologies and cognitive impairment; however, RH significantly increased neuronal hyperactivity and accelerated the progression of cognitive deficits in streptozotocin(STZ)-induced diabetic APP/PS1 mice. GLUT3-mediated neuronal glucose uptake was not significantly altered under hyperglycemia, but was markedly reduced by RH, which induced excessive mitochondrial fission in the hippocampus. Overexpression of GLUT3 specifically in DG area of hippocampus enhanced mitochondrial function and improved cognitive deficits induced by RH. Activation of TRPC6 increased GLUT3-mediated glucose uptake in brain and alleviated RH-induced cognitive deficits, and inactivation of Ca^{2+}/AMPK pathway was responsible for TRPC6-induced GLUT3 inhibition. Taken together, RH impairs brain GLUT3-mediated glucose uptake and further provokes neuronal mitochondrial dysfunction by inhibiting TRPC6 expression, which then accelerates the progression of cognitive deficits in diabetic APP/PS1 mice. Avoiding RH is essential for glycemic control in diabetic patients, and TRPC6/GLUT3 represent potent targets for delaying the onset of dementia in diabetic patients.

Recurrent moderate hypoglycemia accelerates the progression of Alzheimer's disease through impairment of TRPC6/GLUT3 pathway

Authors: Chengkang He[1], Qiang Li[1], Yuanting Cui[1], Peng Gao[1], Wentao Shu[1], Qing Zhou[1], Lijuan Wang[1], Li Li[1], Zongshi Lu[1], Yu Zhao[1], Huan Ma[1], Xiaowei Chen[2], Hongbo Jia[3], Hongting Zheng[4], Gangyi Yang[5], Daoyan Liu[1], Martin Tepel[6] and Zhiming Zhu[1*]

Affiliations:

[1]Department of Hypertension and Endocrinology, Center for Hypertension and Metabolic Diseases, Daping Hospital, Army Medical University, Chongqing Institute of Hypertension, Chongqing 400042, China

[2]Brain Research Center, Army Medical University, Chongqing 400038, China

[3]Suzhou Institute of Biomedical Engineering and Technology, Chinese Academy of Sciences, Suzhou 215000, China

[4]Department of Endocrinology, Translational Research Key Laboratory for Diabetes, Xinqiao Hospital, Army Medical University, Chongqing, China

[5]Endocrine Department, Second Affiliated Hospital of Chongqing Medical University, Chongqing 400010, China

[6]Odense University Hospital, Department of Nephrology, University of Southern Denmark, Institute for Molecular Medicine, Cardiovascular and Renal Research, Institute of Clinical Research, Odense, Denmark.

[*]Correspondence to Zhiming Zhu, Department of Hypertension and Endocrinology, Center for Hypertension and Metabolic Diseases, Daping Hospital, Army Medical

University, Chongqing Institute of Hypertension, Chongqing 400042, China. E-mail: zhuzm@yahoo.com

Abstract

Currently, the most effective strategy for dealing with Alzheimer's disease (AD) is delaying the onset of dementia. Severe hypoglycemia is strongly associated with dementia; however, the effects of recurrent moderate hypoglycemia (RH) on progression of cognitive deficits in diabetic patients with genetic susceptibility to AD remain unclear. Here, we report that insulin-controlled hyperglycemia only slightly aggravated AD-type pathologies and cognitive impairment; however, RH significantly increased neuronal hyperactivity and accelerated the progression of cognitive deficits in streptozotocin(STZ)-induced diabetic APP/PS1 mice. GLUT3-mediated neuronal glucose uptake was not significantly altered under hyperglycemia, but was markedly reduced by RH, which induced excessive mitochondrial fission in the hippocampus. Overexpression of GLUT3 specifically in DG area of hippocampus enhanced mitochondrial function and improved cognitive deficits induced by RH. Activation of TRPC6 increased GLUT3-mediated glucose uptake in brain and alleviated RH-induced cognitive deficits, and inactivation of Ca^{2+}/AMPK pathway was responsible for TRPC6-induced GLUT3 inhibition. Taken together, RH impairs brain GLUT3-mediated glucose uptake and further provokes neuronal mitochondrial dysfunction by inhibiting TRPC6 expression, which then accelerates progression of cognitive deficits in diabetic APP/PS1 mice. Avoiding RH is essential for glycemic control in diabetic patients, and TRPC6/GLUT3 represent potent targets for delaying the onset of dementia in diabetic

patients.

Keywords: Diabetes, Recurrent moderate hypoglycemia, Alzheimer's disease, Glucose Transporter 3, Transient receptor potential cation channel subfamily C member 6

Introduction

Alzheimer's disease (AD) is the most common form of dementia and is characterized by progressive deficits in memory and cognitive function. Clinically, AD may be early-onset familial AD or late-onset sporadic AD, with the latter closely associated with genetic and metabolic risk factors, such as diabetes, hypertension, obesity, smoking, and depression, that significantly exacerbate AD-type pathologies and promote disease progression(1-3). Efficient therapies remain elusive despite intensive research on treatments for AD over the past few decades, and given that the symptoms and pathology of late-onset sporadic AD develop over many years or even decades, control of risk factors is essential to delay or prevent the progression of severe cognitive deficits.

Nevertheless, determinants of accelerated cognitive decline in diabetic patients with genetic susceptibility to AD are less clear because glucose dyshomeostasis is complex and can range from chronic hyperglycemia to treatment-induced recurrent hypoglycemia or be combined with hypertension and cardiovascular complications. Hypoglycemic episodes due to tight glycemic control using insulin or other hypoglycemic agents occur in about 25%-30% of diabetic patients(4, 5). Previous studies have demonstrated that even one episode can induce hypoglycemia-associated autonomic failure and subsequent recurrent hypoglycemia(6, 7). Moderate

hypoglycemia (blood glucose falls to 3.3-2.2 mM) is far more common than severe hypoglycemia (5, 8), and diabetic patients with history of severe hypoglycemia are at higher risk of cognitive impairment and AD (9, 10). However, whether recurrent moderate hypoglycemia (RH) is related to AD progression remains unknown because RH is usually self-remitted and not easily aware. Interestingly, while RH has been reported to exert protective effects on cognition in normal rats and in animals with a history of severe hypoglycemia (11, 12)，contradictory effects were seen in diabetic mice (13), implying heterogeneity in the effects of RH on cognition and reiterating the need to delineate the underlying mechanism(s) to delay onset of dementia in diabetic patients susceptible to AD.

Aerobic oxidation of glucose in the mitochondria is the predominant source of brain ATP. While translocation of glucose across the blood-brain barrier (BBB) and astrocyte plasma membrane is mainly mediated by glucose transporter 1 (GLUT1) (14, 15), glucose uptake into neurons is almost exclusively mediated by GLUT3 (16-18), and the expression of other glucose transporters is much lower than that of either (19). Importantly, glucose transporter expression significantly changes in response to energy demands or under pathophysiological conditions; indeed, brain GLUT1 and GLUT3 protein levels are considerably lower in AD patients and animal models of AD(20) . In STZ-induced diabetic rats, GLUT3 protein expression was specifically upregulated in the hippocampus, whereas GLUT1 protein abundance was similar to that of nondiabetic littermates(21, 22). High-fat diet feeding of mice downregulates glucose transporter (GLUT)-1 expression in blood-brain barrier (BBB)(23). As GLUT-3-mediated glucose

transport into neurons is metabolized in mitochondria to produce ATP, and mitochondrial dysfunction is causally associated with dementia (2, 24, 25), the question is whether RH can affect the expression and function of brain GLUTs and further impair brain mitochondrial function.

The transient receptor potential channel 6 (TRPC6) is a Ca^{2+}-permeable nonselective cation channel whose expression is sensitive to glucose fluctuation (26, 27). We have recently shown that a RH-induced reduction in TRPC6 expression led to cognitive impairment under diabetic conditions by impairing hippocampal mitochondrial function(28). However, it is unknown whether RH similarly promotes the development of cognitive deficits in diabetic APP/PS1 mice. As the expression of GLUTs is markedly regulated by free cytosolic Ca^{2+} and AMPK (29-31), we hypothesized that TRPC6 dysfunction could affect GLUT-mediated glucose uptake. Therefore, this study examined if and how RH participates in the progression of AD-type pathology and cognitive deficits in diabetic APP/PS1 mice.

Results

RH increases neuronal hyperactivity in diabetic APP/PS1 mice

Parameters, such as body weight, blood pressure, random blood glucose (RBG), glucose tolerance, and HbA1c were not significantly different between the APP/PS1-DM and APP/PS1-DM-RH mice (Figure S1A–E). STZ-induced diabetes significantly reduced body weight and glucose tolerance, and increased RBG and HbA1c level (Figure S1A, S1C and S1E), but did not significantly alter blood pressure when compared to APP/PS1 mice (Figure S1B). There were no significant differences

between wild-type (WT) and APP/PS1 groups (Figure S1A–E). During insulin-induced hypoglycemic episodes, blood glucose in the APP/PS1-DM-RH group ranged between 2.2–3.9 mM, which was sustained for about 120 min (Figure S1F).

Spontaneous ongoing neuronal activity is known to be a significant determinant of brain information processing (32, 33), and disturbances in neuronal activity are one of the main functional defects in animal models of AD (34). Here, we employed in vivo two-photon Ca^{2+} imaging of layer 2/3 neurons in the prefrontal cortex (PFC) to reveal the effects of RH on neuronal activity, and show increased frequency of Ca^{2+} transients and greater fraction of hyperactive neurons in 6-month-old APP/PS1 mice compared to WT mice, indicating neuronal hyperactivity without changes in the fraction of silent neurons (Figure 1A–D). In diabetic APP/PS1 mice, the fraction of both silent and hyperactive neurons was higher compared to APP/PS1 mice (Figure 1D). Next, we assessed spontaneous ongoing neuronal activity in APP/PS1-DM-RH mice and found that RH significantly increased the frequency of Ca^{2+} transients (APP/PS1-DM vs APP/PS1-DM-RH, 2.80 ± 0.09 vs 3.20 ± 0.13 transients/min) and fraction of hyperactive neurons (12.60 ± 0.77 (%) vs 17.76 ± 0.97 (%); Figures 1C, D). However, there was no significant difference in the fraction of silent neurons (Figure 1D). Taken together, these results reveal that RH induces neuronal hyperactivity in diabetic APP/PS1 mice.

RH accelerates progression of AD-type pathologies and cognitive deficits

To investigate the direct effect of RH on neuronal morphology，we detected the expression level of neuronal and synaptic markers in the hippocampus. Compared to

WT mice, 6-month-old APP/PS1 mice displayed only mild synaptic loss, as evidenced by negligible differences in positive area fraction of NeuN and MAP2 staining (Figure 2A), or abundance of PSD95 and SYP protein, despite a reduction in SNAP25 expression (Figure 2B). However, hippocampal neuronal and synaptic loss in STZ-induced diabetic APP/PS1 mice was prominent (Figure 2A and 2B). Importantly, the positive area fraction of NeuN and MAP2, along with expression of PSD95, SYP, and SNAP25 protein, were significantly lower in APP/PS1-DM-RH mice compared to APP/PS1-DM mice (Figures 2A, B), indicating that RH significantly aggravates neuronal and dendritic loss.

Next, we evaluated the effects of RH on brain Aβ protein deposition and neuroinflammation. Compared to WT mice, 6-month-old APP/PS1 mice displayed obvious Aβ protein deposition and neuroinflammation in hippocampus, and which was significantly exacerbates by RH in STZ-induced diabetic APP/PS1 mice (Figure S2A–D). Specifically, total amyloid plaques, detected by 6E10 staining, were significantly increased by RH (Figure S2A). ELISA results also indicated a significant increase in the level of Aβ40 and Aβ42 from APP/PS1-DM-RH mice (Figure S2C). Astrocytosis and microgliosis were dramatically enhanced by RH (Figure S2B), as were levels of proinflammatory cytokines, including TNF-α, IFN-γ, IL-1β, and IL-6, in hippocampal homogenates (Figure S2D). These results demonstrate that RH markedly accelerates the progression of AD-type pathologies.

Given these negative effects, on neuronal activity and AD-type pathologies, we further investigated the cognitive sequelae due to RH in STZ-induced diabetic APP/PS1

mice using behavioral tests. WT and 6-month-old APP/PS1 mice performed equally well, while STZ-induced diabetes significantly impaired the performance of APP/PS1 mice (Figure 3A–H). Importantly, the cognitive deficits in STZ-induced diabetic APP/PS1 mice were further aggravated by RH. In Morris water-maze test, APP/PS1-DM-RH mice required a longer latency escape (Figure 3A). The number of center area crossing (Figure 3B) and time spent in quadrant 3 (Figure 3C) by APP/PS1-DM-RH mice were significantly lower than that of APP/PS1-DM mice. In the Y-maze and Open-field tests, APP/PS1-DM-RH mice performed worse than the APP/PS1-DM mice, as reflected by fewer number of entries, lesser time spent in the novel arm (Figure 3D and 3E), shorter center distance traveled, and reduced rearing (Figure 3F–3H). Additionally, we assessed the effects of RH on cognitive function in non-diabetic APP/PS1 mice and results showed that RH treatment significantly impaired the performances of mice in behavioral tests (Figure S3A-S3G). These results indicate that RH significantly promotes the progression of cognitive deficits and accelerates the appearance of the dementia phenotype under diabetic condition.

RH exacerbates brain mitochondrial dysfunction and energy stress

As recurrent glucose deficiency may impair mitochondrial function and ultimately induce energy stress, we used TEM and O2K to observe the morphology and function of hippocampal mitochondria, and demonstrate that mitochondrial morphology and function, along with ATP content, were similar in 6-month-old APP/PS1 mice and WT mice (Figure 4A–F). STZ-induced diabetes only slightly impaired mitochondrial morphology, but it increased expression of p-Drp1 (Ser643) and markedly impaired

both mitochondrial function and ATP content (Figure 4A–F). Importantly, RH led to obvious fragmentation in the hippocampus, as reflected by the reduction in mitochondrial length (major axes) and the ratio of length to width (Figure 4A and 4B). Consistently, the expression of p-Drp1 (Ser 643), MFN1, and MFN2 were significantly reduced while the expression of p-Drp1 (Ser 622) was increased in APP/PS1-DM-RH mice compared to APP/PS1-DM mice, suggesting excessive mitochondrial fission (Figure 4C and 4D). Correspondingly, RH significantly exacerbated the reduction in mitochondrial oxidative phosphorylation and ATP content (Figure 4E and 4F). Thus, these results demonstrate that RH exacerbates brain mitochondrial dysfunction and energy stress in STZ-induced diabetic APP/PS1 mice.

RH reduces GLUT3-mediated glucose uptake in neurons

Next, we investigated the mechanisms underlying such accelerated progression of cognitive deficits in APP/PS1-DM-RH mice. As transporter-mediated brain glucose uptake is the major source of energy for normal neuronal function, we assessed the effect of RH on brain glucose uptake by measuring SUV of ^{18}F-FDG in mice using micro-PET/CT. Interestingly, STZ-induced diabetic APP/PS1 mice showed nearly preserved SUV for ^{18}F-FDG as 6-month-old APP/PS1 mice (Figure 5A and 5B, Figure S4A–S4H). However, SUV was significantly lower after RH in the entire brain of STZ-induced diabetic APP/PS1 mice (Figure 5A and 5B, Figure S4A–S4H) and of non-diabetic APP/PS1mice (Figure S5B–S5O), suggesting that RH impairs brain glucose uptake.

We further sought to identify the glucose transporter that contributes to this

dysfunction, and show that hippocampal expression of GLUT1 and GLUT3 was not changed significantly in APP/PS1 mice compared to WT mice; however, it was dramatically increased in APP/PS1-DM mice. Interestingly, the expression of GLUT1 was further increased while that of GLUT3 was significantly decreased in the APP/PS1-DM-RH group (Figure 5C). The expression of GLUT3 was also reduced in APP/PS1-RH mice when compared with APP/PS1 mice (Figure S5A). Immunofluorescent staining showed that the GLUT3 expression in hippocampal CA1, CA3 and DG region were significantly increased in diabetic APP/PS1 mice, while reduced by RH (Figure S6A–S6C). Expression of other glucose transporters such as SGLT1, SGLT2, GLUT2, GLUT4, and GLUT5, in the hippocampus, either remained unchanged or was not detected after RH (Figure 5C), indicating that a RH-induced reduction in GLUT3 expression contributes to the impairment of neuronal glucose uptake.

GLUT3 over-expression improves RH induced mitochondrial dysfunction and cognitive deficits

To uncover whether hippocampal mitochondrial dysfunction and cognitive deficits caused by RH is causally resulted from the reduction of GLUT3-mediated glucose uptake. We firstly over-expressed GLUT3 in PC12 cells (Figure S7A and S7B) using lentiviral vector and found that it led to significantly increased mitochondrial function and ATP content (Figure S7C and S7D).

Then, an adeno-associated virus (AAV2/9) vector carrying mouse *slc2a3* gen, selectively transducing neurons, was injected into the hippocampal DG area of

4-month-old APP/PS1-DM mice (AAV-GLUT3) and the control group (AAV-Con) received with same dosed of AAV vector. After 3 days of virus injection, these two groups of mice were received RH treatment for 8 weeks. GLUT3 abundance in DG area of AAV-GLUT3 mice (Figure S8A) was significantly higher than that in AAV-Con mice. GLUT3 over-expression markedly reduced the levels of Aβ40 and Aβ42 (Figure S8B) and levels of proinflammatory cytokines, including TNF-α, IFN-γ, IL-1β, and IL-6, in DG area of hippocampus in APP/PS1-DM-RH mice (Figure S8C), indicating that GLUT3 over-expression ameliorates RH induced AD-type pathology. Additionally, the mitochondrial respiratory function and ATP content were significantly increased by GLUT3 overexpression (Figure 6A and 6B). More importantly, we compared performances in behavioral tests between AAV-Con mice and AAV-GLUT3 mice, and results showed that GLUT3 overexpressed APP/PS1-DM-RH mice performed better than control mice in Morris-water maze test (Figure 6C and 6D), Y-maze test (Figure 6E and 6F) and open field test (Figure 6G-I). Taken together, these findings demonstrate that RH accelerates the progression of AD-type pathologies and cognitive deficits in STZ-induced diabetic APP/PS1 mice by inhibiting GLUT3-mediated glucose uptake.

TRPC6 activation enhances GLUT3-mediated glucose uptake in the brain and alleviates RH-induced cognitive deficits

To investigate whether GLUT3 expression was regulated by TRPC6，we firstly measured TRPC6 expression in hippocampus, Western blotting show that TRPC6 expression was significantly increased in APP/PS1-DM mice, but that RH significantly

reduced TRPC6 expression (Figure 7A). There was no significant difference in TRPC6 expression between APP/PS1 and WT mice (Figure 7A). Immunofluorescent staining showed that TPRC6 expression was significantly reduced in hippocampal CA1, CA3 and DG region (Figure S9A–S9C) .Long-term activation of TRPC6 with hyperforin, an agonist of TRPC6, significantly increased GLUT3 expression (Figure 7B) and brain glucose uptake (Figure S10A–S10L), along with mitochondrial function and ATP content in APP/PS1-DM-RH mice (Figure S11A and S11B). More importantly, hyperforin treatment significantly reduced Aβ deposition (Figure S12A), GFAP expression (Figure S12B), levels of IFN-γ, IL-1β, IL-6 and TNFα (Figure S12C), and improved performance in behavioral tests (Figure S13A–S13G), suggesting reversal of cognitive deficits. Injecting adeno-associated virus (AAV2/9) expressing mouse *TRPC6*-specific shRNA (shRNA-TRPC6) into the hippocampal DG area of APP/PS1 mice remarkably reduced the expression of TRPC6, p-AMPKα and GLUT3, while the expression of GLUT1 and GLUT4 were not changed significantly (Figure S14A). Importantly，the spatial memory and exploration ability in shRNA-TRPC6 mice was obviously impaired when compared with shRNA-Con mice (Figure S14B-S14H). In PC12 cells, lentivirus-mediated TRPC6 overexpression (Lv-TRPC6) led to higher ^{18}F-FDG uptake and GLUT3 abundance compared to the control group (Lv-Con), indicating enhanced GLUT3-mediated glucose uptake (Figure 7C and 7D). However, eliminating cytosolic Ca^{2+} with BAPT-AM or inhibiting AMPK activation using compound c, abolished TRPC6 overexpression-induced increase in GLUT3 (Figure 7E and 7F). Further, activating AMPK with AICAR significantly increased GLUT3

expression (Figure 7G), and while RH reduced the expression of p-AMPKα (Thr172) (Figure 7H), hyperforin increased it in hippocampus (Figure 7I). Interestingly, the expression levels of GLUT1, GLUT4, and SGLT1 were not altered significantly by TRPC6 overexpression (Figure S15A and S15B), and the expression of GLUT2, GLUT5, and SGLT2 were not detected in PC12 cells (Figure S15A and S15B). TRPC6 overexpression improved both mitochondrial function and ATP content in PC12 cells (Figure 7J and 7K). Taken together, these results suggest that RH impairs GLUT3-mediated glucose uptake by inhibiting the TRPC6/Ca^{2+}/AMPK pathway, which not only leads to dysfunctional neuronal mitochondrial energy metabolism but also eventually accelerates the progression of cognitive deficits in STZ-induced diabetic APP/PS1 mice (Figure 7L).

Discussion

Here, we demonstrate that 8 weeks of RH treatment dramatically aggravates cortical hyperactivity, that it promotes the progression of cognitive deficits in diabetic APP/PS1 mice, and that it significantly impairs GLUT3-mediated neuronal glucose uptake, which is associated with neuronal TRPC6 dysfunction. These data suggest that RH is a potent risk factor that can facilitate AD development and that TRPC6 might be a potential target for alleviating hypoglycemia-associated cognitive impairment. However, the conclusion in this study was drawn by using STZ-induced type 1 diabetic mice but not using type 2 diabetic animal model, thus these findings may not apply to type 2 diabetic patients.

Diabetes mellitus is highly prevalent worldwide and is recognized as one of the

major risk factors for cognitive decline and AD. Notably, up to half of all AD cases are potentially attributable to modifiable risk factors (e.g., diabetes, hypertension, and obesity) (35) , and although various hypoglycemic drugs have been used to treat diabetes, glycemic control alone fails to prevent cognitive decline in diabetic patients. Thus, it is critical to uncover how disturbances in glucose homeostasis lead to cognitive decline in diabetic patients who are susceptible to AD. Recurrent hypoglycemia is a common complication in diabetic patients, and several clinical trials have demonstrated that even one episode of severe hypoglycemia can significantly increase the risk of dementia in elderly diabetic patients (10, 36, 37). As episodes of moderate hypoglycemia are more frequent and usually imperceptible in diabetic patients, the detrimental effects of RH on the development of AD are frequently neglected. Here, we show that 6-months-old APP/PS1 mice had mild Aβ deposition, negligible neuronal loss and neuro-inflammation, and normal cognitive performances. Diabetic APP/PS1 mice with insulin-controlled hyperglycemia only had slight cognitive deficits. However, 8 weeks of RH treatment dramatically accelerated the progression of AD-type pathologies and cognitive impairment in diabetic APP/PS1 mice, indicating that RH can promote AD progression. In non-diabetic APP/PS1 mice, the cognitive function was also impaired by 8 weeks of RH treatment, which indicates that RH induced cognitive function under non-diabetic condition directly caused by hypoglycemia rather than due to signals that response to hypoglycemia. However, diabetes is a complex clinical syndrome and the cognitive deficits induced by RH may resulted from the glucose-independent effects under

diabetic condition.

Neuronal hyperactivity is an early functional impairment in AD transgenic mice(38), wherein, while Aβ alone promotes hyperactivity, tau suppresses activity and promotes silencing of neurons (34). We show that hyperglycemia increased both neuronal silencing and hyperactivity in APP/PS1 mice but that RH only increased the fraction of hyperactive neurons in diabetic APP/PS1 mice; the latter observation is corroborated by greater Aβ deposition.

Normal neuronal activity is dependent on glucose homeostasis, and its disturbance is one of the major features of AD. Decreased brain glucose metabolism reflects synaptic activity deficit in the brain(39) . However, whole brain glucose uptake was normal in 6-month-old APP/PS1 mice, which concurs with results from previous studies that have reported significant decline in brain glucose uptake in APP/PS1 mice but only at age 12 months. Importantly, our results indicate that while normal brain glucose uptake can be maintained despite underlying hyperglycemia, it is impaired by vigorous fluctuations in brain glucose, as seen during RH.

Glucose is transported across cell membranes by GLUTs and SGLTs and the human brain expresses several GLUT proteins and SGLT proteins. In AD patients, the levels of GLUT1 and GLUT3, the major brain glucose transporters, are decreased in the cerebral cortex(40). In this study, we report that GLUT1 expression in the hippocampus of diabetic APP/PS1 mice is increased by RH, and several studies have revealed that insulin-induced hypoglycemia in diabetic rats increases GLUT1 expression in the BBB, which is essential for maintaining glucose supply required for neurological functions

(41, 42). Given the observed reduction in brain glucose uptake and activated neuro-inflammatory response, we believed that increased GLUT1 expression is due to astrocyte activation, as reflected by enhanced GFAP expression, rather than as a compensatory response to hypoglycemia. One study has reported that hypoglycemia for 8 days increased neuronal GLUT3 expression, reflecting a neuron-specific adaptation against hypoglycemia(43). Here, our results showed that the GLUT3 expression and standard uptake value of FDG were significantly reduced by 8 weeks of RH treatment in APP/PS1 mice and diabetic APP/PS1 mice. We believed that the contradiction of GLUT3 expression and glucose uptake maybe resulted from the intensity of intervention that 8 weeks of RH treatment disturbs the adaption caused by 8 days of provocation. It has also been demonstrated that diabetes causes severe cerebrovascular injury, leading to reduced cerebral blood flow and glucose supply to the brain (44-46). In this study, hippocampal GLUT3 expression in APP/PS1-DM mice were significantly higher than that of APP/PS1 mice, even though glucose uptake remained unchanged, indicating that the increase in GLUT3 expression is an adaptive response to diabetes to maintain adequate neuronal glucose supply; however, RH disturbs this adaptation in diabetic APP/PS1 mice. Thus, even though GLUT3 expression in APP/PS1-DM-RH mice was comparable to that of WT and APP/PS1 mice, glucose uptake was significantly reduced. Additionally, we can't rule out the possibility that the impaired glucose uptake resulted from neuro-inflammation and neuronal loss caused by RH.

Transporter-mediated glucose delivery to neurons is predominantly diverted to the mitochondria for ATP production; thus, its recurrent shortage may trigger mitochondrial

dysfunction and cause brain energy stress. Indeed, ATP production from glucose metabolism declines dramatically in late-onset sporadic AD, and this tendency continues throughout the progression of the disease(47, 48). We show that RH induced hippocampal mitochondrial fragmentation, which was substantiated by the reduction in MFN1, MFN2, and p-Drp1 (Ser 643) abundance, along with cognate reduction in oxidative phosphorylation and ATP content. GLUT3 over-expression significantly enhanced glucose uptake, mitochondrial function and ATP content in PC12 cells. Thus, excessive hippocampal mitochondrial fission caused by RH could be a response to glucose shortage caused by impairment of GLUT3-mediated glucose uptake in diabetic APP/PS1 mice. However, the mechanisms underlying changes in MFN1/2 expression and Drp1 activity require further investigation.

We have recently reported that TRPC6 is a critical sensitive cation channel to hypoglycemia and a promising target for preventing RH-induced cognitive impairment (28). Here, we extend these observations and link the TRPC6/Ca^{2+}/AMPK pathway and GLUT3 expression in APP/PS1-DM-RH mice, i.e., that RH reduces hippocampal TRPC6/AMPKα/GLUT3 expression but that hyperforin-induced long-tern activation of TRPC6 reverses this effect and delays the onset of severe cognitive impairment. Similar results were seen with PC12 cells as GLUT3 expression was significantly inhibited by BAPT-AM and Compound C, but increased upon AMPK activation by AICAR. We recently showed that GLP-1 receptor agonist, liraglutide, can improve the cognitive function in patients with type 2 diabetes mellitus (49). Thus, the protective effects of hyperforin on cognitive function should be further tested in diabetic patients. Taken

together, we show that hyperglycemia only slightly impairs cognitive function but that RH significantly promotes the progression of AD by inhibiting TRPC6/GLUT3-mediated glucose uptake in diabetic APP/PS1 mice. Activation of TRPC6 with hyperforin could delay the present of dementia caused by RH. Therefore, we propose that hypoglycemic treatment in diabetic patients with AD risk should adopt the "better high than low" strategy to avoid recurrent episodes of moderate hypoglycemia.

Materials and Methods

STZ-induced diabetic APP/PS1 mice. APP/PS1 transgenic mice and wild-type mice (C57BL/6) were purchased from Junke biological Co (Nanjing, China) and bred in the animal room of the institute. To establish the diabetic model, streptozotocin (50 mg/kg/day) was injected (i.p.) for consecutive 5 days in 4-month-old male APP/PS1 mice. At 3 days after the final injection, mice with random blood glucose (RBG) ≥16.7 mM were defined as STZ-induced diabetic APP/PS1 mice (APP/PS1-DM). To ensure animal health and to replicate blood glucose control in diabetic patients, diabetic mice were administrated insulin (glargine) once a day. The starting dose of 3 IU/kg was injected subcutaneously, and the dose was adjusted according to the glucose levels. All procedures followed guidelines issued by the University Animal Welfare Committee.

RH and Hyperforin treatment. Hypoglycemia (2.2–3.9 mM) was induced in 4-month-old mice in the APP/PS1-DM group by injecting regular insulin (i.h., 5.0 units/kg, started at 15:00) thrice/week. This was continued for a period of 8 weeks, i.e., until the animals were 6 months old (APP/PS1-DM-RH). Blood glucose level was

monitored using a glucometer, each hypoglycemia episode was maintained for about 2 hours, and mice were subsequently provided free access to food to restore glycemic status. If blood glucose was lower than 2.2 mM, glucose (1g, intragastric) was immediately administered to avoid severe hypoglycemia. Mice that suffered severe hypoglycemia were excluded from the study. Some RH-treated mice were administrated hyperforin (6 mg/kg, i.p., sigma, PHL89225) for 8 weeks (APP/PS1-DM-RH-Hyp). All the mice in the control group were similarly treated with saline. One week after completion of RH treatment, all animals underwent behavioral tests followed by ^{18}F-FDG PET/CT and two-photon imaging. All these procedures were conducted under euglycemic conditions.

^{18}F-FDG PET/CT imaging Glucose uptake in the brain and in PC12 cells was assessed on a Micro-PET-CT scanner (Pingseng Healthcare Co, China). On the day of experiment, STZ-induced diabetic APP/PS1 mice were not treated with insulin. Specifically, mice were anesthetized with isoflurane and injected with ^{18}F-FDG (about 8 MBq, i.v.) after fasting for 12 h. PC12 cells were seeded in 6-well plates and incubated with ^{18}F-FDG (10 μCi per well) in low-glucose medium at 37°C for 45 min. PET images, 10-min dynamic three-dimensional scans with an energy window of 350–650 keV, were acquired and computed tomography (CT) was used to obtain anatomical reference images. Uptake rates of ^{18}F-FDG were analyzed as volumes of interest (VOIs) drawn over the entire brain. Rate of glucose utilization was measured using standard uptake values (SUV = [^{18}F-FDG activity in each VOI (Bq/ml)] / [injected dose in Bq] / [body weight (g)]).

Behavioral tests. Animals underwent behavioral testing, namely, the Morris-water maze, the Y-maze, and open-field testing, for evaluation of spatial learning, memory, and exploration ability. Three days prior test, mice were brought to the test room for adaptation. In the open-field test, mice were placed in the center of the apparatus and allowed free exploration for 5 min. Paths were recorded and parameters, such as total distance traveled and distance in central area, were measured. In the Y-maze test, mice were allowed to move freely in two arms (home arm and familiar arm) with the other arm (novel arm) blocked for 3 min. After a 2 h interval, mice were allowed to freely explore all three arms for 5 min, and the number of novel arm entries and time spent in the novel arm were recorded. The Morris-water-maze test was conducted on a trial platform and comprised four platform tests per day for 4 consecutive days with a probe trial on the 5^{th} day. Swimming capabilities of the animals were evaluated before the test.

In vivo two-photon Ca^{+2} imaging. All procedures were performed as described in previous study (50). Briefly, animals were anesthetized by inhalation of 1.5%. After removing the skin, a customized recording chamber with a hole at the front was cemented to the skull with cyanoacrylic glue (UHU, Buhl-Baden, Germany). Next, a small craniotomy (1.5×1.5mm) was created at the projecting point of the frontal cortex (1.5 mm lateral to the middle and 2.9 mm anterior to the bregma), bleeding was stopped and 1.5% agarose was layered on the exposed cortex to suppress pulsation. Respiration rate was maintained between 90 and 110 /per min. Neurons in layer 2/3 of the prefrontal cortex were bulk loaded with 0.5 mM Ca^{2+} indicator Cal-520 AM (AAT-Bioquest, Sunnyvale, CA) under the two-photon microscope. Imaging was performed on a

two-photon microscope with a 12-kHz resonant scanner (model “LotosScan 1.0,” Suzhou Institute of Biomedical Engineering and Technology). A laser source provided excitation light (λ = 920 nm; Coherent, Mountain View, CA) through a water-immersion objective (Nikon, 40X, NA 0.8) and a consecutive recording (4–6 min) was acquired at a 40-Hz frame rate using custom-written software based on LabVIEW (National Instruments). Data analysis was performed using LabVIEW 2014 (National Instruments) and Igor Pro 5.0 (Wavemetrics). Glial cells were excluded based on morphology and time course of Ca^{2+} transients.

Stereotactic Injection. AAV2/9 vectors carrying shRNA targeting mouse *Trpc6* (AAV2/9-H1-shRNA-CAG-EGFP-WPRE-pA, shRNA-TRPC6, Taitool Biotechnology Co., Ltd) or mouse *slc2a3* gen (AAV2/9-hSyn-EGFP-P2A-slc2a3-3xflag-WPRE, AAV-GLUT3) and control virus (shRNA-Con, AAV-Con) were bilaterally injected into the hippocampus DG region of APP/PS1 mice or diabetic APP/PS1 mice, respectively. Specifically, the mice were fixed in the stereotaxic apparatus and anesthetized with isoflurane. Then, , a small craniotomy was created at the projecting point of the DG region (AP = −1.9; ML = ± 1.1; DV = − 2.0). Virus was injected at a speed of 0.1 μL/min with Hamilton needle by using an automatic microinjection system (World Precision Instruments) and the needle was left in the injection point for 10 min before slowly retracted. After 3 days of injection, mice from AAV-con and AAV-GLUT3 group were received RH treatment. After 4 weeks of injection, mice from shRNA-Con and shRNA-TRPC6 group were performed behavioral.

Histopathological staining. Free-floating 12 mm serial coronal sections of the

brain were cut on a freezing microtome (Leica) and washed three times. For immunofluorescent staining, sections were blocked with Immunol Staining Blocking Buffer and incubated with primary antibody (anti-NeuN (ab177487, abcam), anti-MAP-2 (ab5392, abcam), anti-GFAP (ab7260, abcam)，anti-GLUT3(Alomone lab, GTX129175), anti-TRPC6 (Millipore, T6442)) overnight at 4 °C. After washing, sections were incubated with secondary antibody diluted in Secondary Antibody Dilution Buffer (Beyotime, China) for 45 min at 37℃. Anti-beta amyloid antibody (abcam, ab2539) and anti-Iba1 antibody (abcam, ab178847) was used for beta amyloid and Iba1 visualization. Images were acquired on a Leica laser confocal microscope or an optical microscope, and area fraction of positive staining against area of tissue analyzed in the neocortex and the hippocampus were quantified using ImageJ software.

ELISA. Animals were sacrificed and the brain was quickly harvested, and the hippocampus homogenized in liquid nitrogen. Concentrations of Aβ40, Aβ42 (R&D Systems, DAB140B, DAB142), HbA1c (MSK, kt20296), IL-6, IL-1β, INF-γ, and TNF-α (Boster, EK0411, EK0394, EK0375, EK0527, respectively) in tissue homogenate was quantitatively measured by ELISA according to manufacturer's instructions.

Mitochondrial morphology, function, and ATP content. Hippocampal morphology was assessed using transmission electron microscopy (TEM), and about 100 mitochondria per sample were used for morphometry. Mitochondria from tissue or cells were extracted using the Mitochondria Isolation Kit (Beyotime) and high-resolution respirometry (O2K) was used to measure respiratory function, as previously described

(28). ATP content was determined using the Enhanced ATP Assay Kit (Beyotime).

Cell culture and Lentiviral infection. Well-differentiated PC12 cells were purchased from Procell (China) and cultured in DMEM medium supplemented with 10% FBS and 1% streptomycin/ penicillin. Recombinant lentivirus vector (Ubi-MCS-3FLAG-SV40-EGFP-IRES-puromycin), purchased from GENECHEM (Shanghai, China), was used for TRPC6 or GLUT3 overexpression. To evaluate the role of Ca^{2+} signaling, BAPT-AM (2μM, Ca^{2+} chelator), Compound C (10 μM, MCE), or AICAR (1 mM, MCE) was added.

Western blot. Hippocampal tissues or cells were homogenized in buffer (0.5 mol/L Tris, 1% NP40, 1% Triton X-100, 1 g/L sodium dodecyl sulfate, 1.5 mol/L NaCl, 0.2 mol/L EDTA, 0.01 mol/L EGTA, and protease inhibitor and/or phosphatase inhibitor), sonicated, and incubated at −20℃ for 20 minutes, followed by centrifugation at 12000*g* for 20 minutes at 4°C. The supernatant was collected and protein concentration determined by the BCA method. Next, 50 μg protein was loaded on 10% SDS polyacrylamide gel. The primary antibodies used were, including anti-TRPC6 (ACC-017, alomone), anti-PSD 95 (ab238135, abcam), anti-SNAP25(ab109105, abcam), anti-SYP (ab32127, abcam), anti-MFN1 (ab126575, abcam), anti-MFN2 (ab124773, abcam), anti-Drp1(ab184247, abcam), anti-p-Drp1(mice Ser 622, 3455, CST), anti-p-Drp1(mice Ser 643, ab193216, abcam), anti-GLUT1-5 antibody (AF6731, DF7510, AF5463, AF5386, DF13545,Affinity), anti-SGLT1 (PA5-77460, Invitrogen) and anti-SGLT2 (ab137207, abcam), and followed by incubated with the secondary antibodies (ZSGB-BIO). Protein expression was normalized to GAPDH intensity or

total protein content.

Statistical Analysis. Data are expressed as mean ± SEM. Statistical differences were assessed using the 2-tailed Student's *t*-test, one-way or two-way analysis of variance with Bonferroni's multiple comparison post hoc tests, as appropriate. All analyses were conducted on SPSS 17.0, or GraphPad Prism software, version 6.0 (GraphPad Software). Two-sided P values less than 0.05 were regarded as statistically significant.

Study approval. Procedures were carried out with the approval of, and in accordance with, the Animal Ethics Committee at the Army Medical University, Chongqing.

Author's contributions

Z.Z. initiated the project. Z.Z., C.H. designed the experiments. Z.Z., C.H. wrote the paper. Q.Z., P.G. contributed to experiments. C.H., Y.Z., Q.L., L.L. and Y.C. collected and provided clinical data. C.H., H.M., L.W. and Z.L. analyzed data. X.C., H.J., G.Y., M.T., H.Z., D.L. and Z.Z. critically read and revised the paper. All authors read and approved the manuscript.

Acknowledgments

We thank Tingbing Cao, Aidi Mou for their technical assistance and Prof. Yizheng Wang (Academy of Military Medical Sciences) for his critical suggestion.

Funding

This study was supported by grants from the Funds for Creative Research Groups of China (81721001), Major International (Regional) Joint Research Project (81920108010)

of China and the National Natural Science Foundation of China (81900761, 81770416, 81670382).The funders had no role in the design and conduct of the study; collection, management, analysis, and interpretation of the data; and preparation, review, or approval of the manuscript.

Conflict of interest

The authors have declared that no conflict of interest exist

REFERENCES

1. Wingo TS, et al. Autosomal recessive causes likely in early-onset Alzheimer disease. *Arch Neurol.* 2012;69(1):59-64.
2. Silva MVF, et al. Alzheimer's disease: risk factors and potentially protective measures. *J Biomed Sci.* 2019;26(1):33.
3. Alfaro FJ, et al. White matter microstructure and cognitive decline in metabolic syndrome: a review of diffusion tensor imaging. *Metabolism.* 2018;78:52-68.
4. Donnelly LA, et al. Frequency and predictors of hypoglycaemia in Type 1 and insulin-treated Type 2 diabetes: a population-based study. *Diabet Med.* 2005;22(6):749-55.
5. Languren G, et al. Neuronal damage and cognitive impairment associated with hypoglycemia: An integrated view. *Neurochem Int.* 2013;63(4):331-43.
6. Cryer PE. Mechanisms of sympathoadrenal failure and hypoglycemia in diabetes. *J Clin Invest.* 2006;116(6):1470-3.
7. Lin YY, et al. Risk factors for recurrent hypoglycemia in hospitalized diabetic patients admitted for severe hypoglycemia. *Yonsei Med J.* 2010;51(3):367-74.
8. Lucidi P, et al. Prevention and Management of Severe Hypoglycemia and Hypoglycemia Unawareness: Incorporating Sensor Technology. *Curr Diab Rep.* 2018;18(10):83.
9. Chen YX, et al. Effect of recurrent severe hypoglycemia on cognitive performance in adult patients with diabetes: A meta-analysis. *J Huazhong Univ Sci Technolog Med Sci.* 2017;37(5):642-8.
10. Haroon NN, et al. Risk of dementia in seniors with newly diagnosed diabetes: a population-based study. *Diabetes Care.* 2015;38(10):1868-75.
11. McNay EC, and Sherwin RS. Effect of recurrent hypoglycemia on spatial cognition and cognitive metabolism in normal and diabetic rats. *Diabetes.* 2004;53(2):418-25.
12. Puente EC, et al. Recurrent moderate hypoglycemia ameliorates brain damage and cognitive dysfunction induced by severe hypoglycemia. *Diabetes.* 2010;59(4):1055-62.
13. Zhou Y, et al. Recurrent nonsevere hypoglycemia exacerbates imbalance of mitochondrial homeostasis leading to synapse injury and cognitive deficit in diabetes. *Am J Physiol Endocrinol Metab.* 2018;315(5):E973-E86.
14. Wang L, et al. Glucose transporter 1 critically controls microglial activation through facilitating glycolysis. *Mol Neurodegener.* 2019;14(1):2.
15. Yu S, and Ding WG. The 45 kDa form of glucose transporter 1 (GLUT1) is localized in oligodendrocyte and astrocyte but not in microglia in the rat brain. *Brain Res.* 1998;797(1):65-72.
16. Apelt J, et al. Insulin-sensitive GLUT4 glucose transporters are colocalized with GLUT3-expressing cells and demonstrate a chemically distinct neuron-specific localization in rat brain. *J Neurosci Res.* 1999;57(5):693-705.
17. Choeiri C, et al. Immunohistochemical localization and quantification of glucose transporters in the mouse brain. *Neuroscience.* 2002;111(1):19-34.
18. Mantych GJ, et al. Cellular localization and characterization of Glut 3 glucose transporter isoform in human brain. *Endocrinology.* 1992;131(3):1270-8.
19. Koepsell H. Glucose transporters in brain in health and disease. *Pflugers Arch.* 2020;472(9):1299-343.

20. Gluchowska K, et al. Expression of glucose transporters in human neurodegenerative diseases. *Biochem Biophys Res Commun.* 2021;540:8-15.
21. Reagan LP, et al. Localization and regulation of GLUTx1 glucose transporter in the hippocampus of streptozotocin diabetic rats. *Proc Natl Acad Sci U S A.* 2001;98(5):2820-5.
22. Reagan LP, et al. Neurological changes induced by stress in streptozotocin diabetic rats. *Ann N Y Acad Sci.* 1999;893:126-37.
23. Jais A, et al. Myeloid-Cell-Derived VEGF Maintains Brain Glucose Uptake and Limits Cognitive Impairment in Obesity. *Cell.* 2016;166(5):1338-40.
24. Briston T, and Hicks AR. Mitochondrial dysfunction and neurodegenerative proteinopathies: mechanisms and prospects for therapeutic intervention. *Biochem Soc Trans.* 2018;46(4):829-42.
25. Tobore TO. On the central role of mitochondria dysfunction and oxidative stress in Alzheimer's disease. *Neurol Sci.* 2019;40(8):1527-40.
26. Liu D, et al. High glucose enhances transient receptor potential channel canonical type 6-dependent calcium influx in human platelets via phosphatidylinositol 3-kinase-dependent pathway. *Arterioscler Thromb Vasc Biol.* 2008;28(4):746-51.
27. Sonneveld R, et al. Glucose specifically regulates TRPC6 expression in the podocyte in an AngII-dependent manner. *Am J Pathol.* 2014;184(6):1715-26.
28. He C, et al. Low-glucose-sensitive TRPC6 dysfunction drives hypoglycemia-induced cognitive impairment in diabetes. *Clin Transl Med.* 2020;10(6):e205.
29. Dai W, et al. GLUT3 induced by AMPK/CREB1 axis is key for withstanding energy stress and augments the efficacy of current colorectal cancer therapies. *Signal Transduct Target Ther.* 2020;5(1):177.
30. Vaeth M, et al. Store-Operated Ca(2+) Entry Controls Clonal Expansion of T Cells through Metabolic Reprogramming. *Immunity.* 2017;47(4):664-79 e6.
31. Weisova P, et al. Regulation of glucose transporter 3 surface expression by the AMP-activated protein kinase mediates tolerance to glutamate excitation in neurons. *J Neurosci.* 2009;29(9):2997-3008.
32. Busche MA, et al. Clusters of hyperactive neurons near amyloid plaques in a mouse model of Alzheimer's disease. *Science.* 2008;321(5896):1686-9.
33. Andalman AS, et al. Neuronal Dynamics Regulating Brain and Behavioral State Transitions. *Cell.* 2019;177(4):970-85 e20.
34. Busche MA, et al. Tau impairs neural circuits, dominating amyloid-beta effects, in Alzheimer models in vivo. *Nat Neurosci.* 2019;22(1):57-64.
35. Barnes DE, and Yaffe K. The projected effect of risk factor reduction on Alzheimer's disease prevalence. *Lancet Neurol.* 2011;10(9):819-28.
36. Whitmer RA, et al. Hypoglycemic episodes and risk of dementia in older patients with type 2 diabetes mellitus. *JAMA.* 2009;301(15):1565-72.
37. Feinkohl I, et al. Severe hypoglycemia and cognitive decline in older people with type 2 diabetes: the Edinburgh type 2 diabetes study. *Diabetes Care.* 2014;37(2):507-15.
38. Busche MA, et al. Critical role of soluble amyloid-beta for early hippocampal hyperactivity in a mouse model of Alzheimer's disease. *Proc Natl Acad Sci U S A.* 2012;109(22):8740-5.
39. Mosconi L. Brain glucose metabolism in the early and specific diagnosis of Alzheimer's disease. FDG-PET studies in MCI and AD. *Eur J Nucl Med Mol Imaging.* 2005;32(4):486-510.

40. Simpson IA, et al. Decreased concentrations of GLUT1 and GLUT3 glucose transporters in the brains of patients with Alzheimer's disease. *Ann Neurol.* 1994;35(5):546-51.
41. Kumagai AK, et al. Upregulation of blood-brain barrier GLUT1 glucose transporter protein and mRNA in experimental chronic hypoglycemia. *Diabetes.* 1995;44(12):1399-404.
42. Simpson IA, et al. Blood-brain barrier glucose transporter: effects of hypo- and hyperglycemia revisited. *J Neurochem.* 1999;72(1):238-47.
43. Uehara Y, et al. Chronic insulin hypoglycemia induces GLUT-3 protein in rat brain neurons. *Am J Physiol.* 1997;272(4 Pt 1):E716-9.
44. Chau ACM, et al. Impaired cerebral blood flow in type 2 diabetes mellitus - A comparative study with subjective cognitive decline, vascular dementia and Alzheimer's disease subjects. *Neuroimage Clin.* 2020;27:102302.
45. Iadecola C. The pathobiology of vascular dementia. *Neuron.* 2013;80(4):844-66.
46. van Sloten TT, et al. Cerebral microvascular complications of type 2 diabetes: stroke, cognitive dysfunction, and depression. *Lancet Diabetes Endocrinol.* 2020;8(4):325-36.
47. Szablewski L. Glucose Transporters in Brain: In Health and in Alzheimer's Disease. *J Alzheimers Dis.* 2017;55(4):1307-20.
48. Cadonic C, et al. Mechanisms of Mitochondrial Dysfunction in Alzheimer's Disease. *Mol Neurobiol.* 2016;53(9):6078-90.
49. Li Q, et al. Activation of Glucagon-Like Peptide-1 Receptor Ameliorates Cognitive Decline in Type 2 Diabetes Mellitus Through a Metabolism-Independent Pathway. *J Am Heart Assoc.* 2021;10(14):e020734.
50. Jia H, et al. In vivo two-photon imaging of sensory-evoked dendritic calcium signals in cortical neurons. *Nat Protoc.* 2011;6(1):28-35.

Figures and Figure legends

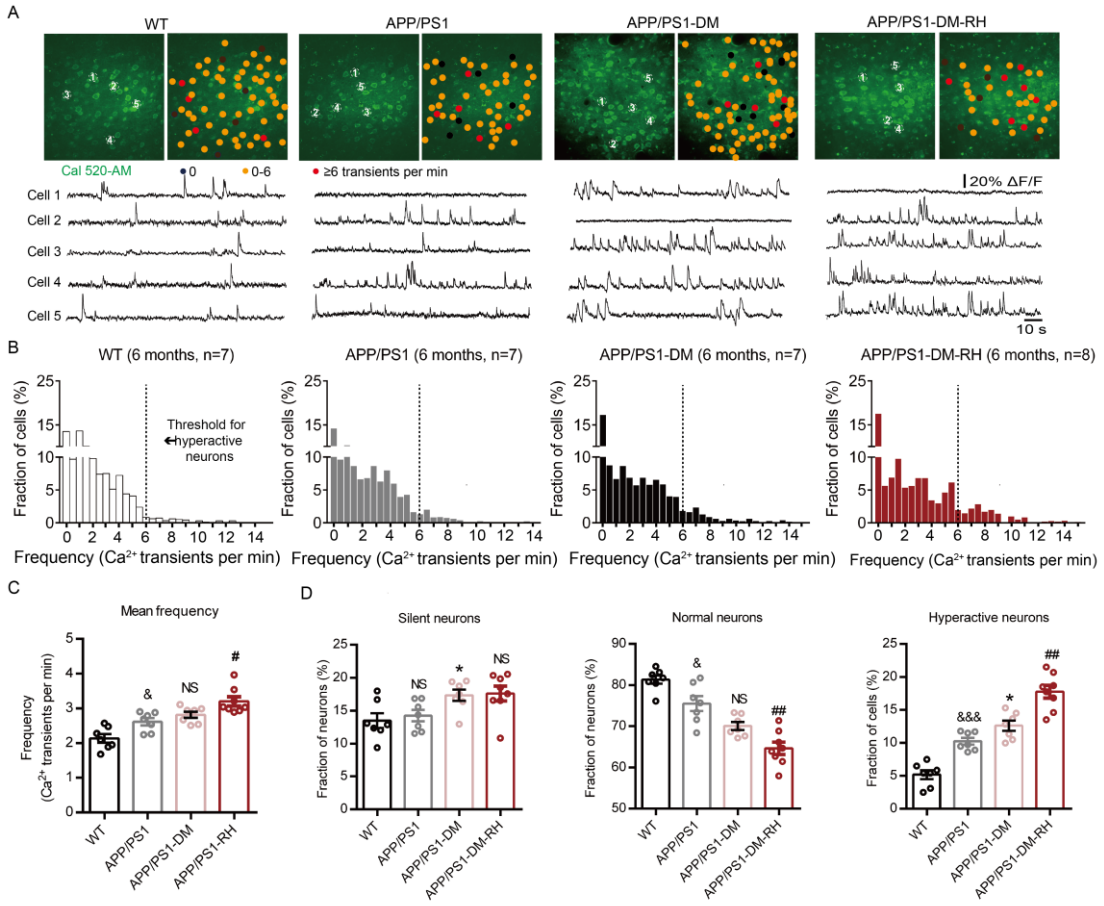

Figure 1. Neuronal hyperactivity in diabetic APP/PS1 mice was significantly increased by RH. (A) ***Top***, representative in vivo two-photon Ca^{2+} images of Cal 520 loading (green) layer 2/3 neurons in the prefrontal cortex from a 6-month-old wild type (WT), APP/PS1, STZ-induced diabetic APP/PS1 (APP/PS1-DM) and recurrent moderate hypoglycemia-treated STZ-induced diabetic APP/PS1 mice (APP/PS1-DM-RH). Neurons were color-coded according to their mean activity. *Black*, silent neurons (0 transients per min); *Orang*e, normal neurons; *Red*, hyperactive neurons ($\geqslant$ 6 transients per min). ***Bottom***, spontaneous Ca^{2+} transients of soma indicated in the top panel. **(B)** Frequency distributions of recorded neurons from WT (n=417 neurons in 7 mice), APP/PS1 (n=376 neurons in 7 mice), APP/PS1-DM (n=411 neurons in 7 mice), and APP/PS1-DM-RH (n=446 neurons in 8 mice) mice. The dashed line serves as the threshold for hyperactive neurons. **(C)** Mean neuronal frequencies for WT (2.136 ± 0.1226 transients per min), APP/PS1 (2.571 ± 0.1177 transients per min), APP/PS1-DM (2.814 ± 0.08978) transients per min, and APP/PS1-DM-RH (3.199 ± 0.1310 transients per min). **(D)** Fraction of silent, normal and hyperactive neurons from indicated groups. The data are expressed as the mean ± SEM. The differences between groups were assessed by one-way ANOVA followed by Dunnett's multiple comparisons test. $^{*}P<0.05$, APP/PS1-DM VS APP/PS1; $^{\&}P<0.05$ and $^{\&\&\&}P<0.001$, WT VS APP/PS1; $^{\#}P<0.05$ and $^{\#\#}P<0.01$, APP/PS1-DM VS APP/PS1-DM-RH; APP/PS1 VS APP/PS1-DM; NS, no significant difference.

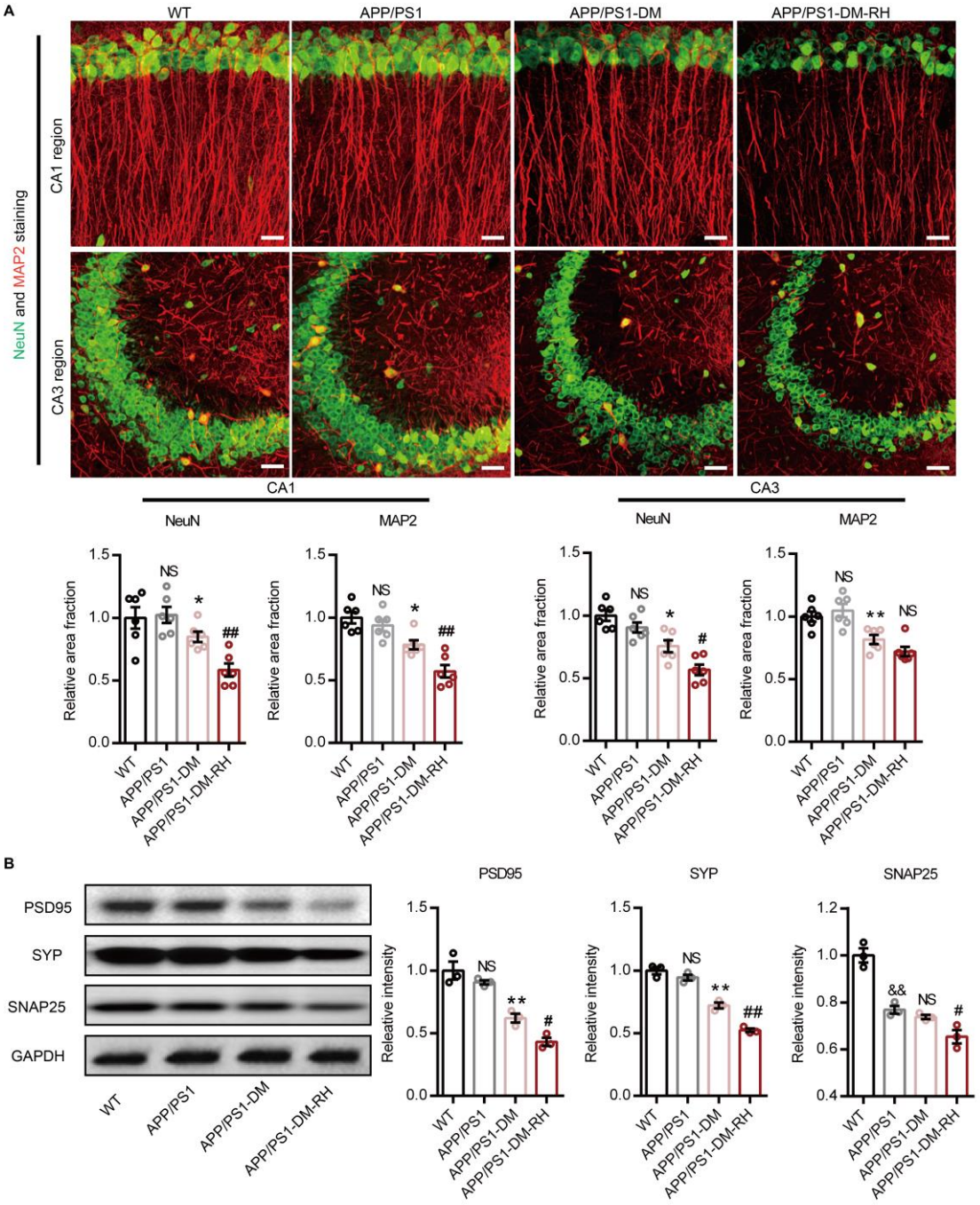

Figure 2. RH exacerbates neuronal injury in hippocampus of diabetic APP/PS1 mice. (A) Representative images of NeuN (green) and MAP2 (Red) immunostaining in CA1 (*top*) and CA3 (*bottom*) region of hippocampus in WT, APP/PS1, APP/PS1-DM, and APP/PS1-DM-RH mice. *Scale bar*, 100μm. Quantitative results are showed in the bottom of images (n=4 mice for each group). (B) Western blot and quantitation for synapse-associated proteins including PSD95, synaptophysin (SYP), and synaptosomal-associated protein 25 (SNAP25) in hippocampal homogenates (n=3 mice for each group). The data are expressed as the mean ± SEM. Statistical significance was assessed using unpaired student's T test. $^{*}P<0.05$ and $^{**}P<0.01$, APP/PS1-DM VS APP/PS1; $^{\#}P<0.05$ and $^{\#}P<0.01$, APP/PS1-DM VS APP/PS1-DM-RH; WT VS APP/PS1, no significant difference (NS).

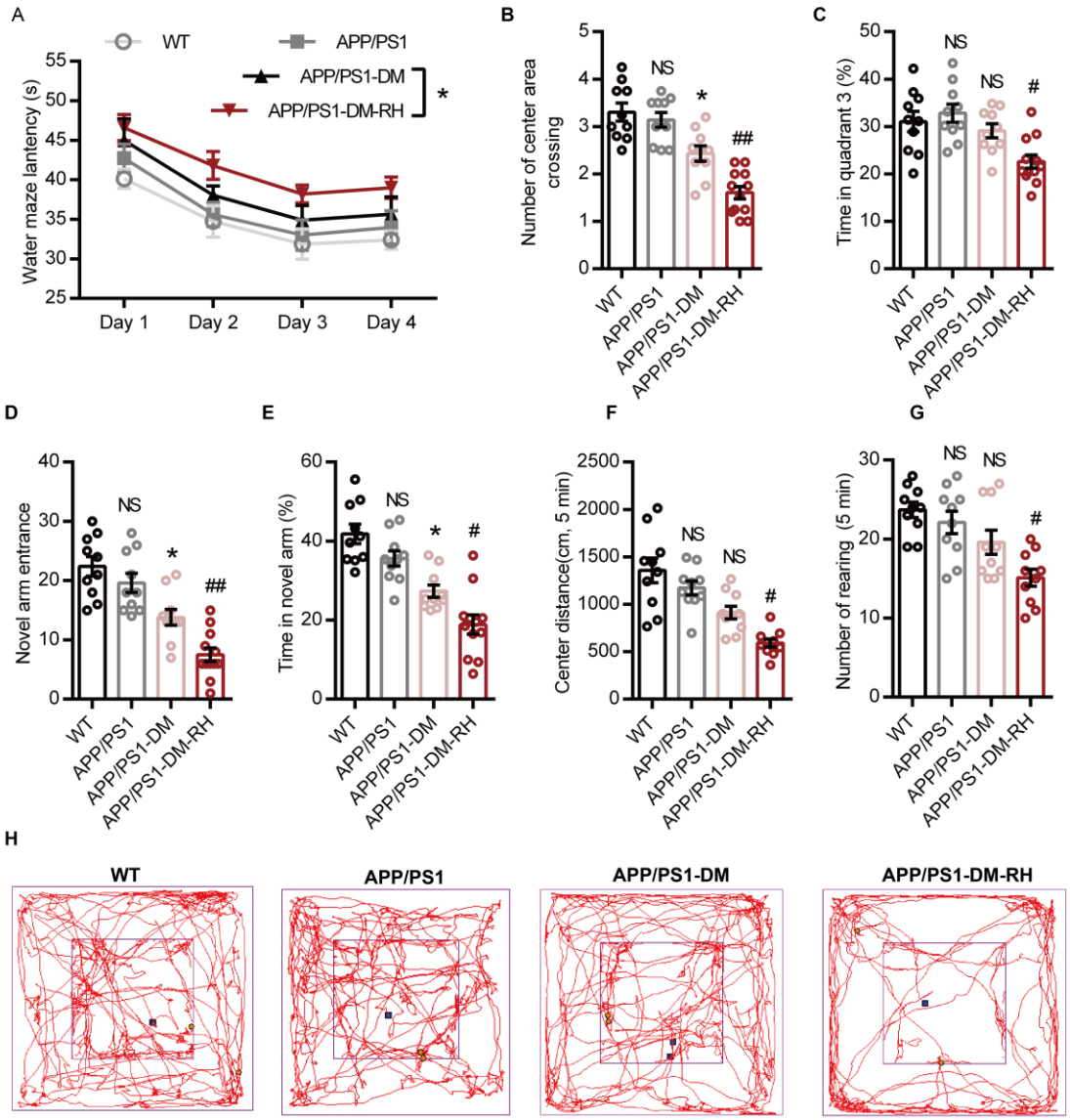

Figure 3. RH aggravates the impairment of behavioral performance in diabetic APP/PS1 mice. (A-C) Morris water-maze test. Escape latency during platform trials (A), number of center area (where the hidden platform had previously been located) crossing (B) and time spend in quadrant 3 of water maze (Q3, C) in probe test. **(D and E)** Novel arm entrance (D) and time spend in the Novel arm (E) in Y-maze test. **(F-H)** Distance traveled in center region (F), number of rearing (G), and representative tracing graphs in open field test (H). n=10-12 mice for each group. The data are expressed as the mean ± SEM. Statistical significances were assessed using one-way ANOVA (panel B-G) or two-way ANOVA (panel A) followed by Dunnett's multiple comparisons test. $^{*}P<0.05$ and $^{**}P<0.01$, APP/PS1-DM VS APP/PS1; $^{\#}P<0.05$ and $^{\#}P<0.01$, APP/PS1-DM VS APP/PS1-DM-RH; WT VS APP/PS1, no significant difference (NS).

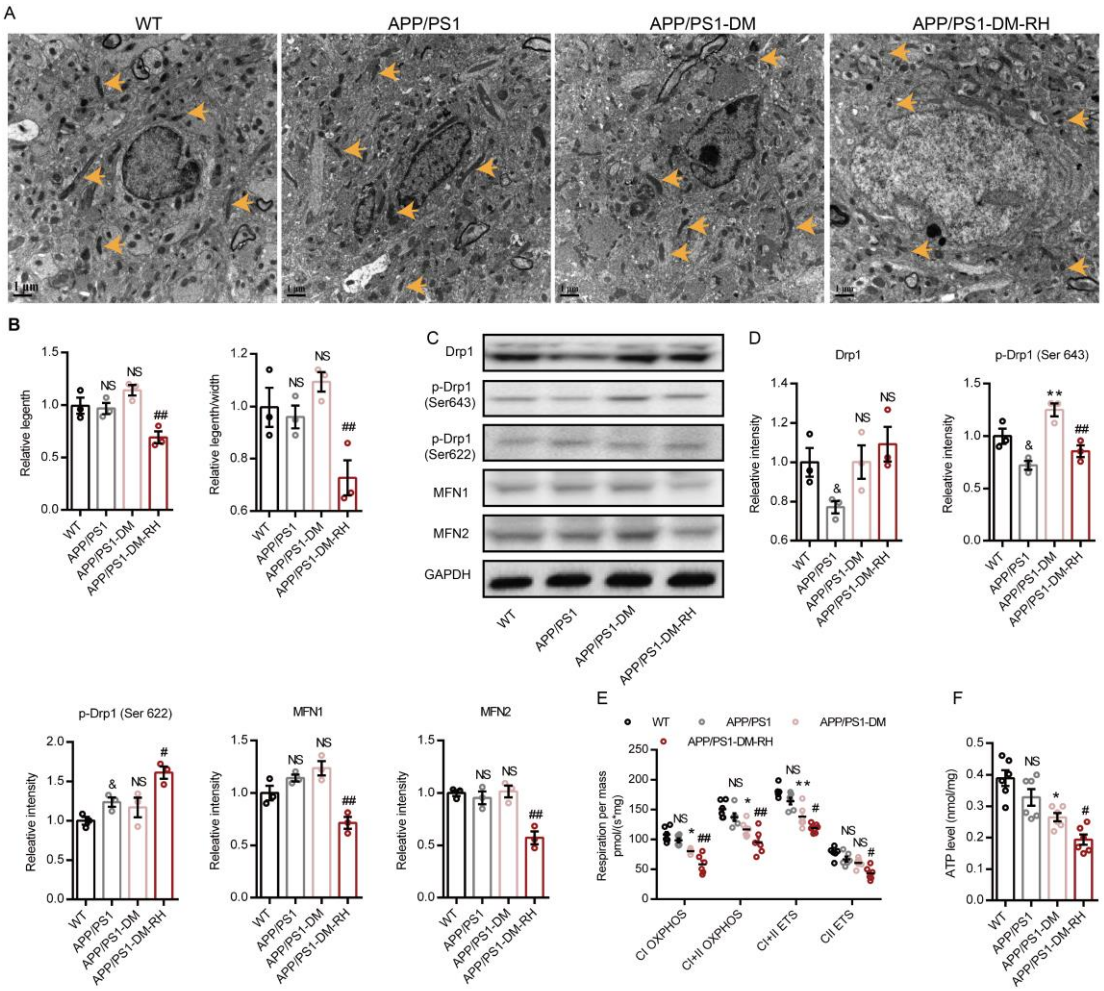

Figure 4. RH exacerbates brain mitochondrial dysfunction and energy stress in STZ-induced diabetic APP/PS1 mice (A and B) Transmission electron microscope (TEM) images showing the mitochondrial morphology (indicated by yellow arrows) in CA1 region of hippocampus (A). Quantitative data of mitochondrial length and ratio of length to width are shown in B (n=200-300 mitochondria, 3 mice for each group). **(C and D)** Western blot images (C) and quantitation (D) for Drp1, MFN1, MFN2, p-Drp1 (Ser 643) and p-Drp1 (Ser 622) in hippocampal homogenates (n=3 mice for each group). **(E)** High-resolution respirometry measured the oxygen consumption capacity of hippocampal mitochondria (n=6 mice for each group). CI OXPHOS, complex I oxidative phosphorylation capacity; CI+CII OXPHOS, complex I plus II oxidative phosphorylation capacity; CII ETS, complex II electron transfer system capacity; CI+CII ETS, complex I plus II electron transfer system capacity. **(F)** ATP content of hippocampus (n=6 mice for each group). The data are expressed as the mean ± SEM. Statistical significance was assessed using unpaired student's t test (panel D) or one-way ANOVA (panel B and F) or two-way ANOVA (panel E) followed by Dunnett's multiple comparisons test or. $^{\&}P<0.05$, WT VS APP/PS1; $^{*}P<0.05$ and $^{**}P<0.01$, APP/PS1-DM VS APP/PS1; $^{\#}P<0.05$ and $^{\#\#}P<0.01$, APP/PS1-DM-RH VS APP/PS1-DM. NS, no significant difference.

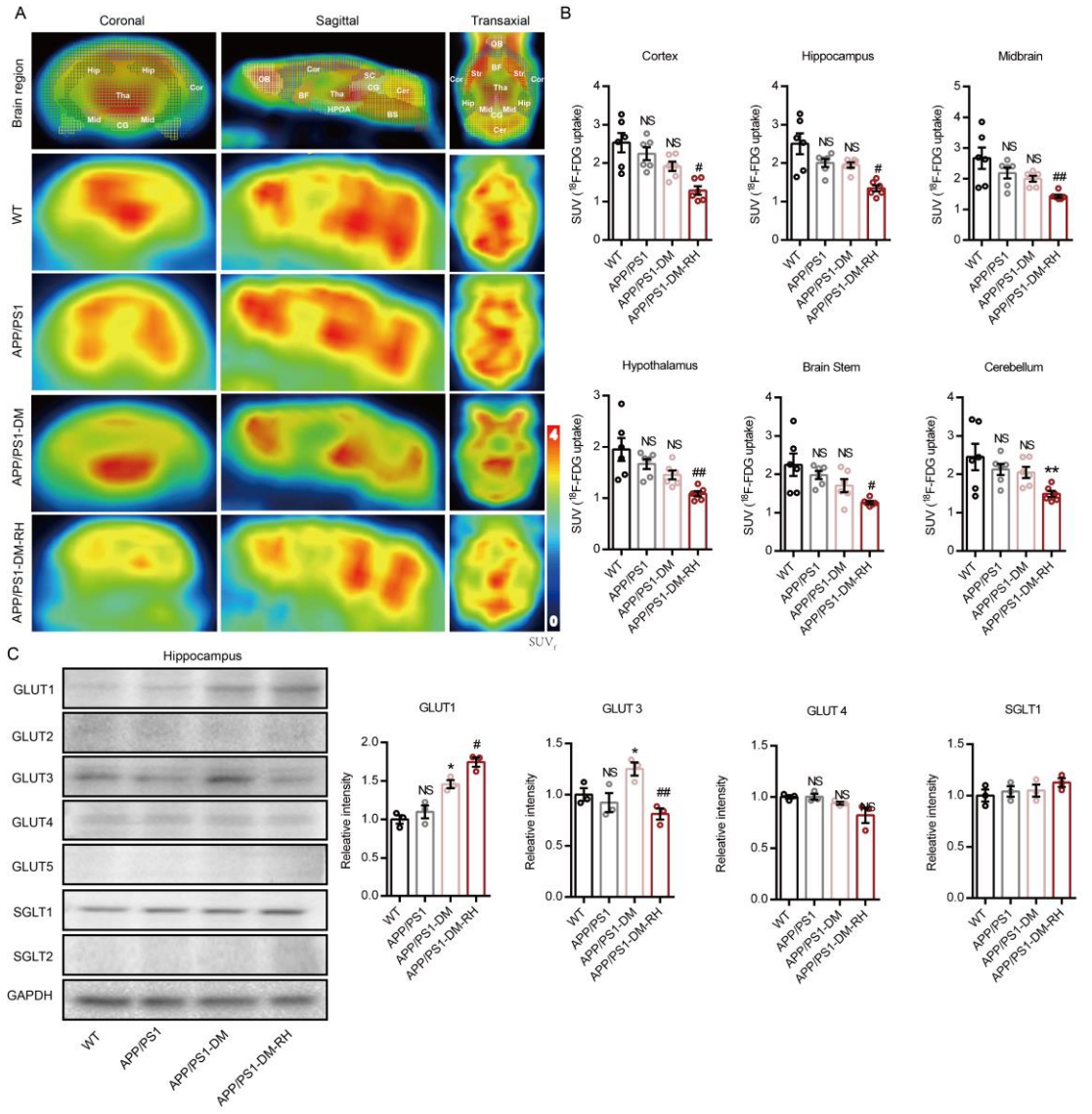

Figure 5. RH reduced brain GLUT3-mediated glucose uptake in STZ-induced diabetic APP/PS1 mice. (A) Representative PET/CT images showing in vivo brain ^{18}F-FDG uptake (coronal, sagittal and transaxial section, n=6 mice for each group). Cor, Cortex; Hip, hippocampus; Mid, midbrain; HPOA, hypothalamus; BS, brain stem; Cer, cerebellum; OB, Olfactory Bulb; BF, basal forebrain; Tha, thalamus; SC, superior colliculi; CG, central gray; Str, striatum. **(B)** Quantification for standard uptake value of ^{18}F-FDG (SUV) in brain region (n=6 for mice for each group). **(C)** Western blot and quantitation for GLUT1, GLUT2, GLUT3, GLUT4, GLUT5, SGLT1 and SGLT2 in hippocampal homogenates (n=3 mice for each group). The data are expressed as the mean ± SEM. Statistical significance was assessed using unpaired student's t test. $^{*}P<0.05$, APP/PS1-DM VS APP/PS1; $^{\#}P<0.05$ and $^{\#}P<0.01$, APP/PS1-DM-RH VS APP/PS1-DM; WT VS APP/PS1, no significant difference (NS).

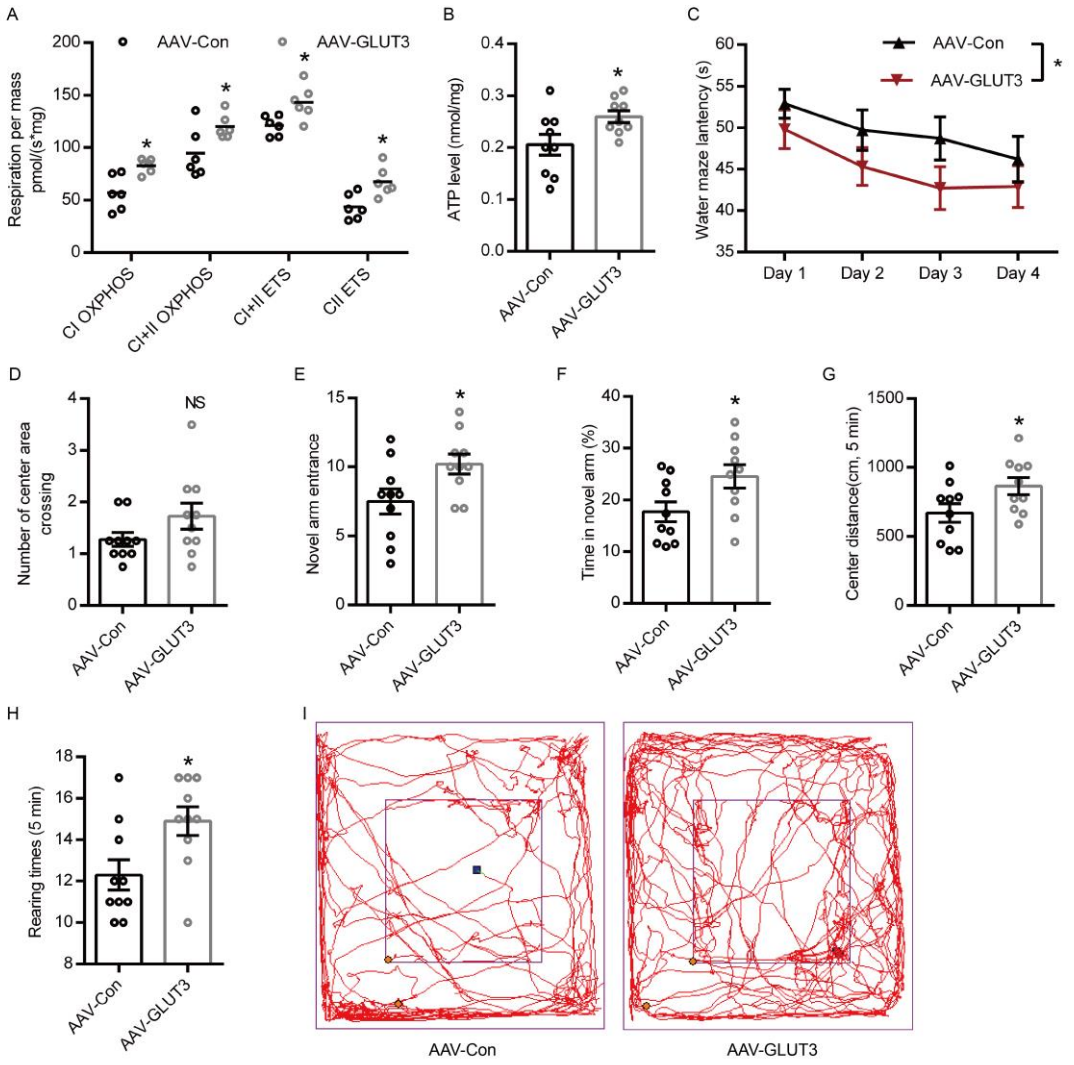

Figure 6. GLUT3 restoration improves mitochondrial dysfunction and cognitive deficits in APP/PS1-DM-RH mice. (A) High-resolution respirometry measured the oxygen consumption capacity of hippocampal mitochondria (n=6 mice for each group). **(B)** ATP content of hippocampus (n=9 mice for each group). **(C and D)** Morris water-maze test. Escape latency during platform trials (C) and number of center area crossing (D) in probe test. **(E and F)** Novel arm entrance (E) and time spend in the Novel arm (F) in Y-maze test. **(G-I)** Distance traveled in center region (H) and number of rearing (G), representative tracing graphs in open field test (I). n=10 mice for each group. The data are expressed as the mean ± SEM. Statistical significances were assessed using two-way ANOVA followed by Sidak's multiple comparisons test (panel A and C) or unpaired student's t test (panel B, D-H). $^{*}P<0.05$.

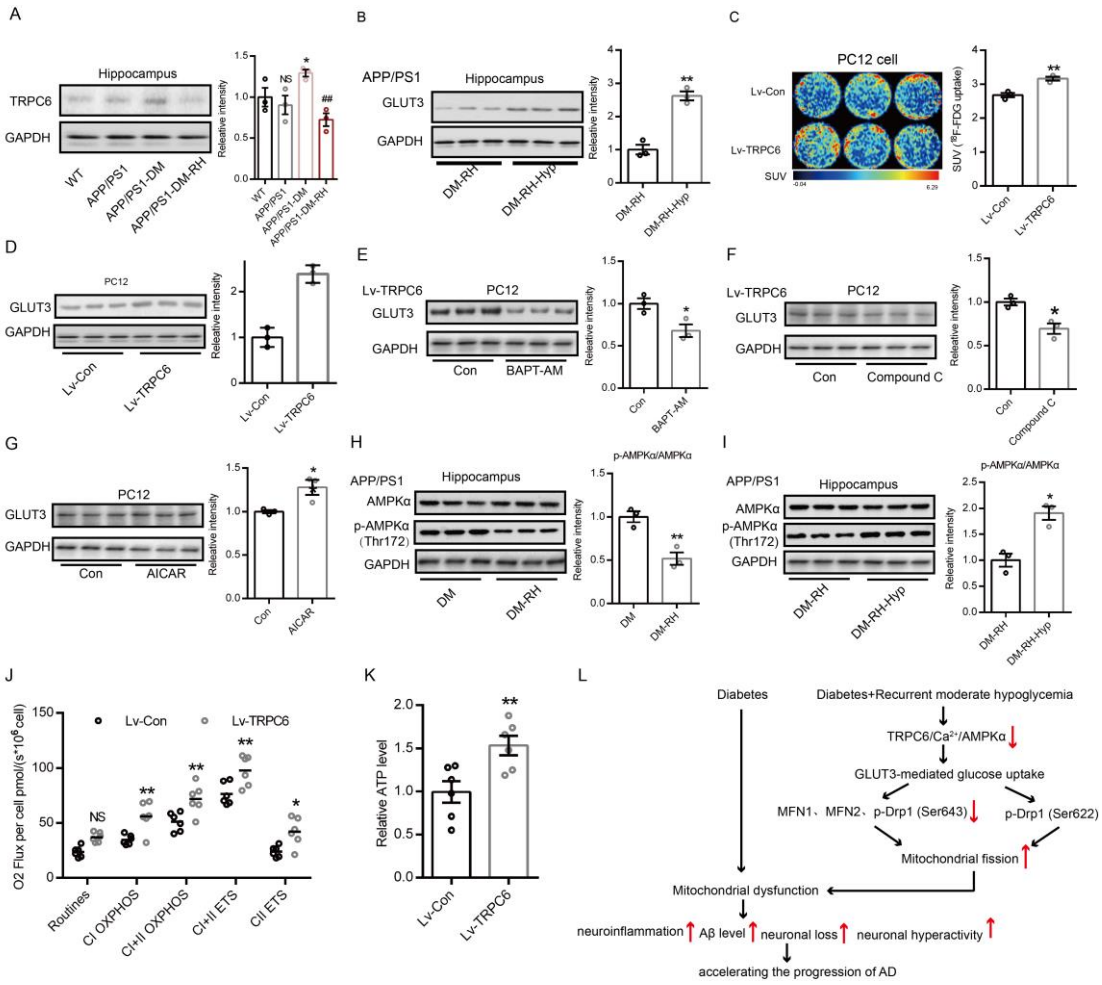

Figure 7. TRPC6 regulates GLUT3-mediated glucose uptake and mitochondrial function. (A and B) Western blot and quantitation for TPRC6 expression (A) and GLUT3 expression (B) in hippocampus (n=3 mice for each group). **(C)** Representative images for glucose uptake measured by ^{18}F-FDG PET/CT scanning in PC12 cells. Standard uptake value (SUV) of ^{18}F-FDG is showed on the right (n=3 for each group). Lv-Con, the recombinant lentiviral vector; Lv-TRPC6, the recombinant lentiviral vector with TRPC6 over-expression. **(D)** Western blot and quantitation for GLUT3 expression in PC 12 cells with or without TRPC6 expression (n=3 for each group). **(E and F)** Western blot and quantitation for GLUT3 expression in TRPC6 over-expressed PC 12 cells treated with BAPT-AM (E, 2 uM) or Compound C (F, 10 uM); **(G)** Western blot and quantitation for GLUT3 expression in PC 12 cells treated with AICAR (1mM). **(H)** Western blot and quantitation for hippocampal AMPKα and p-AMPKα (Thr172) expression in diabetic APP/PS1 mice with or without RH treatment (n=3 mice for each group). **(I)** Western blot and quantitation for hippocampal AMPKα and p-AMPKα (Thr172) expression in diabetic APP/PS1-DM-RH mice with or without hyperforin treatment (n=3 mice for each group). **(J and K)** The mitochondrial respiratory function and ATP level in PC12 cells (n=6 for each group). **(L)** A schematic diagram of this work. The data are expressed as the mean ± SEM. Statistical significance was assessed using unpaired student's T test (panel A-I and K) or two-way ANOVA followed by Sidak's multiple comparisons test (panel J) or one-way ANOVA. $^{*}P<0.05$, $^{**}P<0.01$.

Supplementary figures and legends

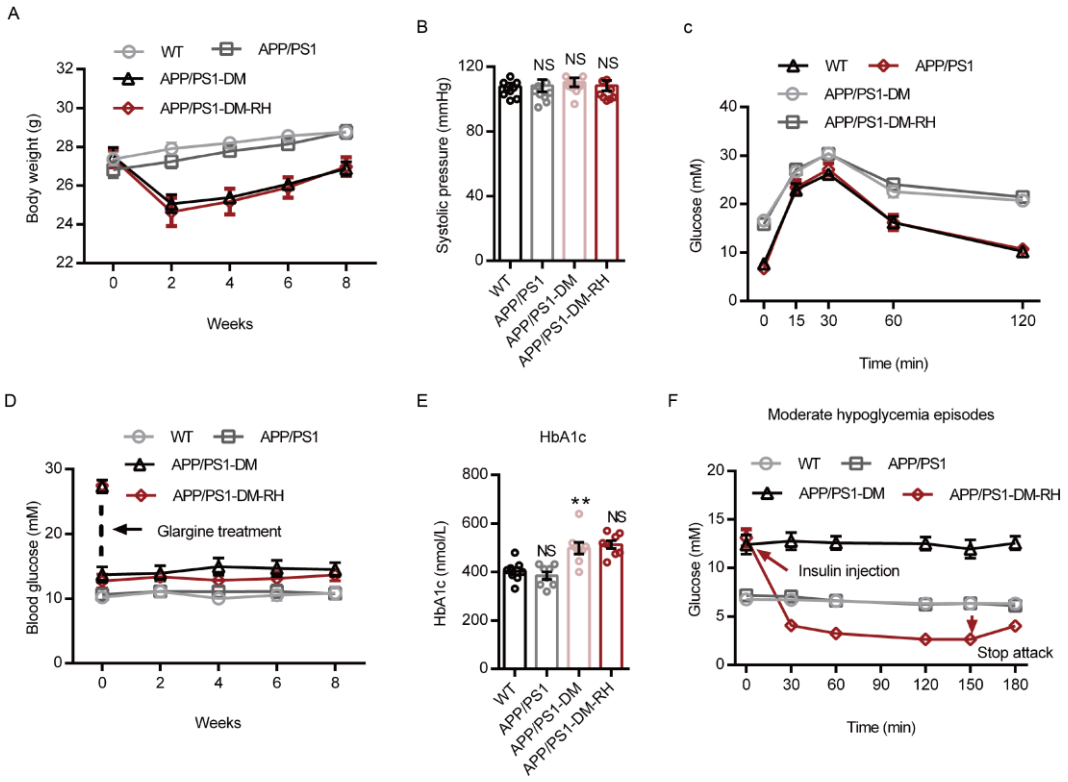

Figure S1, Related to Figure 1. The metabolic effects of RH. (A) Changes of body weight (n=10). **(B)** Blood pressure after completing RH treatment (n=10). **(C)** Intraperitoneal Glucose Tolerance Test (IPGTT) in mice after completing RH treatment (n=6). **(D)** The random blood glucose among 8 weeks of RH treatment (n=10). Glargine treatment, diabetic mice received glargine once a day. **(E)** The HbA1c in serum of mice (n=8 for each group). **(F)** Changes of blood glucose during a moderate hypoglycemia episode induced by insulin injection (n=10).The data are expressed as the mean ± SEM. Statistical significance was assessed using a one-way ANOVA (panel B and E) or two-way ANOVA (panel A, C and D) followed by Dunnett's multiple comparisons test. $^{***}P < 0.001$, APP/PS1-DM VS APP/PS1; WT VS APP/PS1, APP/PS1-DM-RH VS APP/PS1-DM, no significant difference (NS).

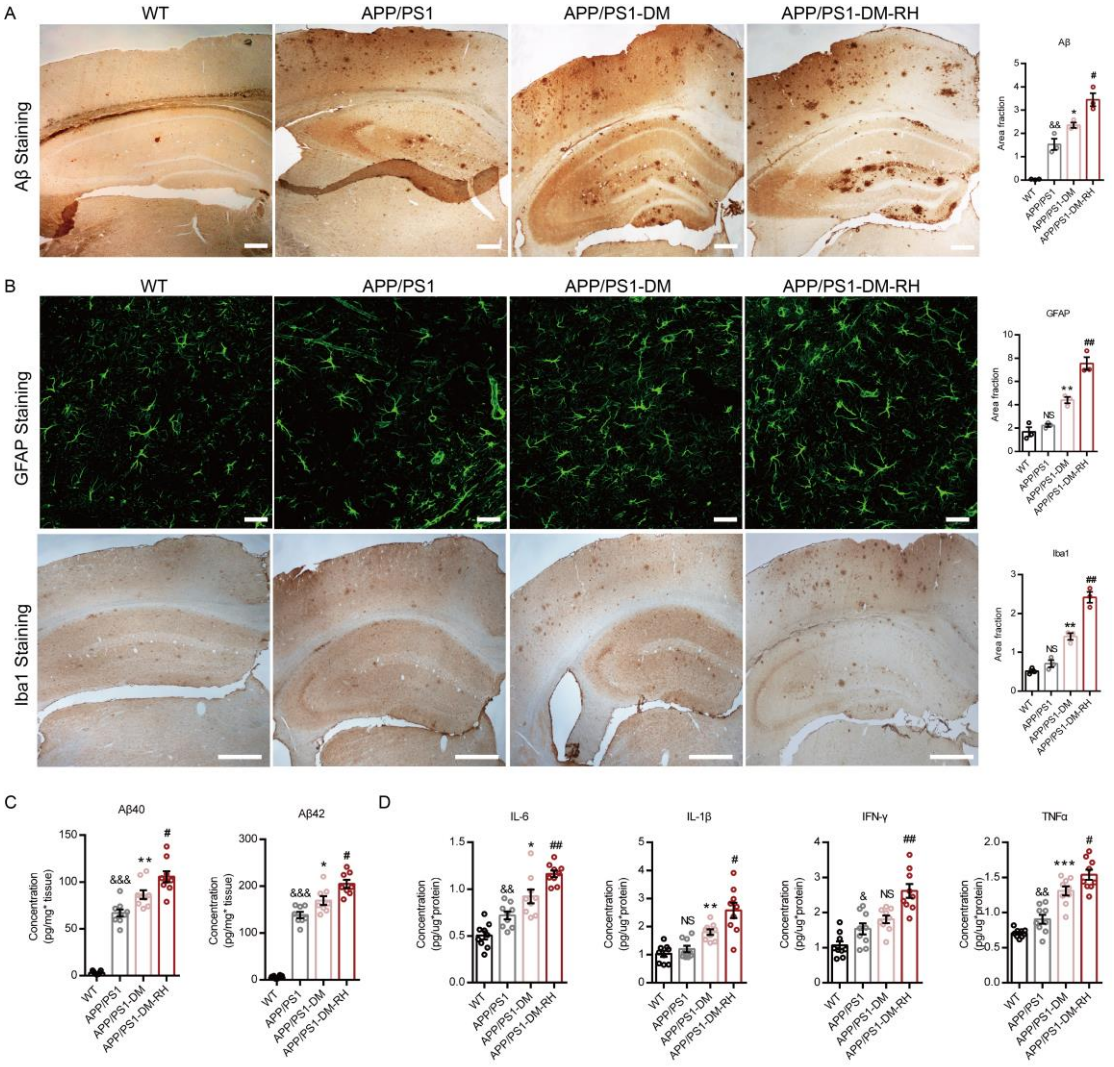

Figure S2, Related to Figure 2. AD-type pathology in hippocampus. (A) Immunohistochemical staining for Aβ deposition in hippocampus. Quantitation is shown on the right (n=3 mice for each group). **(B)** Immunofluorescent staining for GFAP (astrocyte marker, *top*) and immunohistochemical staining for Iba1 (microglia marker, *bottom*). Quantitation is shown on the right (n=3 mice for each group). **(C)** ELISA of Aβ40 and Aβ42 concentration in hippocampal homogenates (n=9 mice for each group). **(D)** Quantification of IL-6, IL-1β, IFN-γ and TNF-α by ELISA in hippocampal homogenates (n=9 mice for each group). The data are expressed as the mean ± SEM. Statistical significance was assessed using unpaired student's T test (panel A-C) one-way ANOVA followed by Dunnett's multiple comparisons test (panel D). $^{\&}P<0.05$ and $^{\&\&}P<0.05$, WT VS APP/PS1; $^{*}P<0.05$, $^{**}P<0.01$ and $^{***}P<0.01$, APP/PS1-DM VS APP/PS1; $^{\#}P<0.05$ and $^{\#\#}P<0.01$, APP/PS1-DM-RH VS APP/PS1-DM; NS, no significant difference.

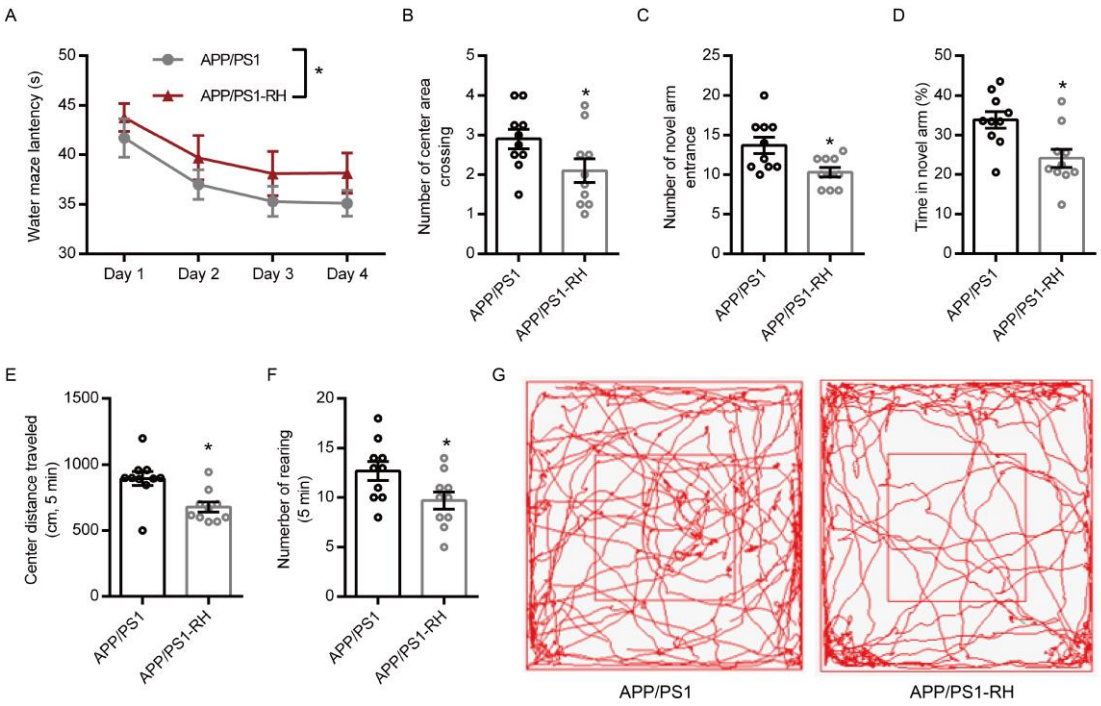

Figure S3, Related to Figure 3. RH impaired the performances of non-diabetic APP/PS1 mice in behavioral tests. (A and B) Morris water-maze test. Escape latency during platform trials (A) and number of center area crossing (B) in probe test. APP/PS1-RH, APP/PS1 mice received 8 weeks of RH treatment. **(C and D)** Novel arm entrance (C) and time spend in the novel arm (D) in Y-maze test. **(E-G)** Distance traveled in center area (E), number of rearing (F), and representative tracing graphs in open field test (G). n=10 for each group. The data are expressed as the mean ± SEM. Statistical significances were assessed using two-way ANOVA (panel A) or unpaired student's T test (panel B-F). $^{*}P<0.05$, $^{**}P<0.01$ versus APP/PS1.

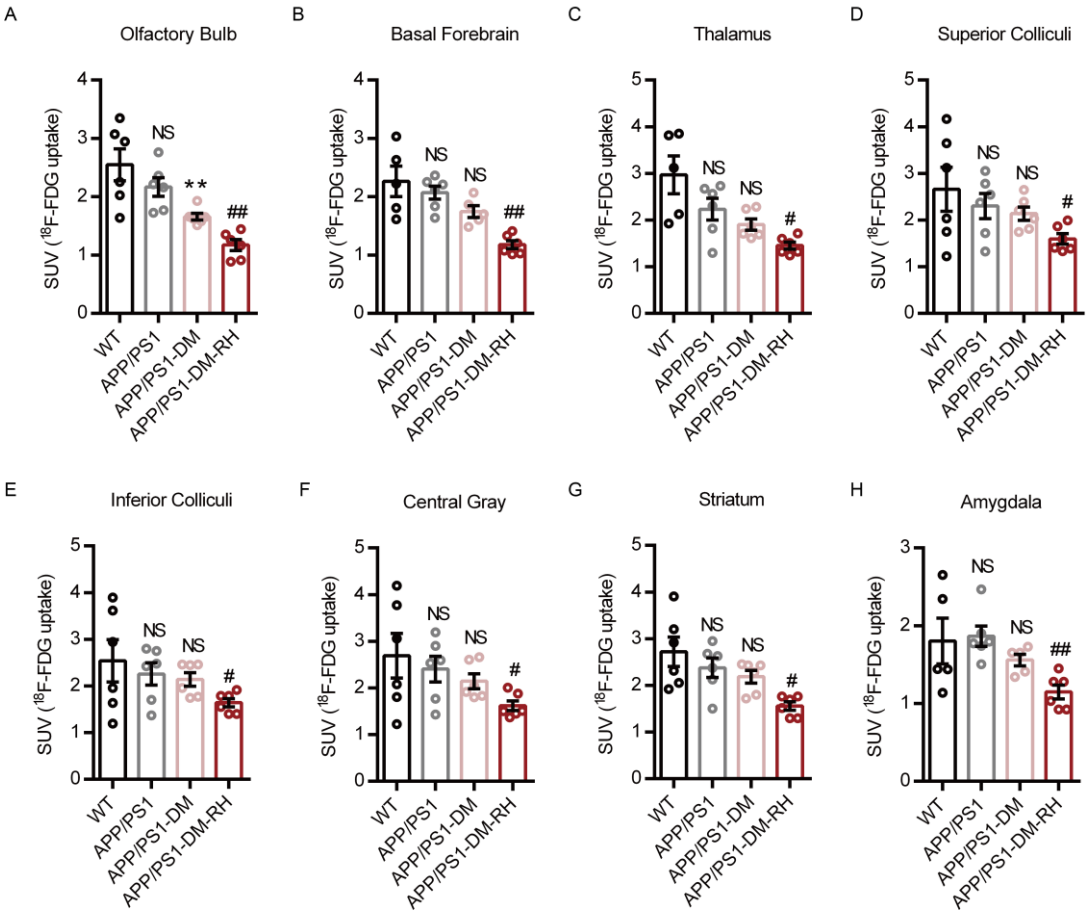

Figure S4, Related to Figure 5. ^{18}F-FDG uptake in brain. (A-H) 18F-FDG uptake in different brain regions measured by PET/CT scanning (n=6 mice for each group). The data are expressed as the mean ± SEM. Statistical significance was assessed using unpaired student's T test. $^{**}P<0.01$, APP/PS1-DM VS APP/PS1; $^{\#}P<0.05$ and $^{\#\#}P<0.01$, APP/PS1-DM-RH VS APP/PS1-DM; WT VS APP/PS1, no significant difference (NS).

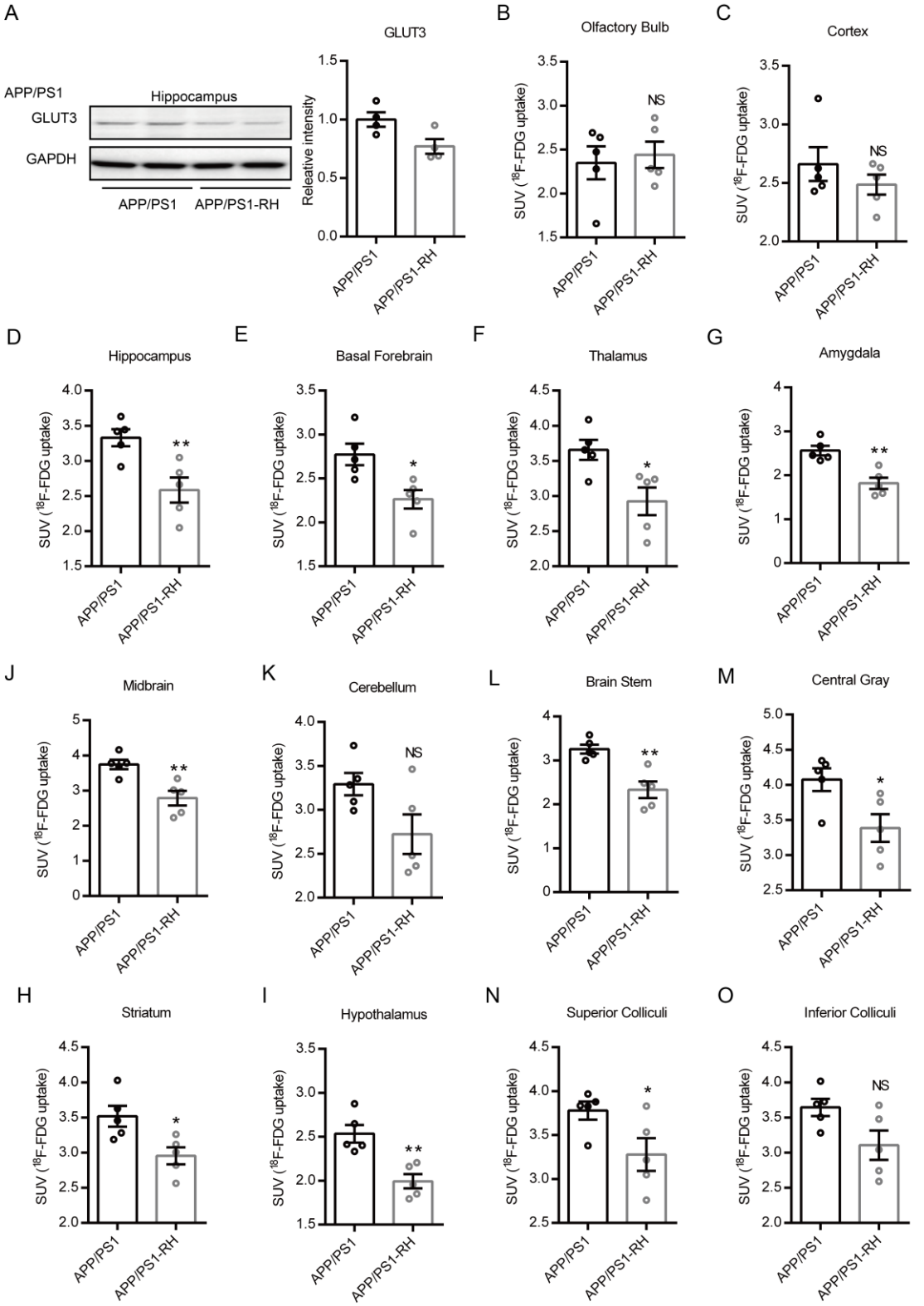

Figure S5, Related to Figure 5. RH reduced hippocampal GLUT3 expression and brain ^{18}F-FDG uptake in non-diabetic APP/PS1 mice. (A) Western-blotting and quantitative data shown the expression of hippocampal GLUT3 (n=4 mice for each group). APP/PS1-RH, APP/PS1 mice received 8 weeks of RH treatment. **(B-O)** The standard uptake value (SUV) of ^{18}F-FDG in brain area (n=5 mice for each group). The data are expressed as the mean ± SEM. Statistical significance was assessed using unpaired student's T test. *P＜0.05,**P＜0.01; NS, no significant difference (NS).

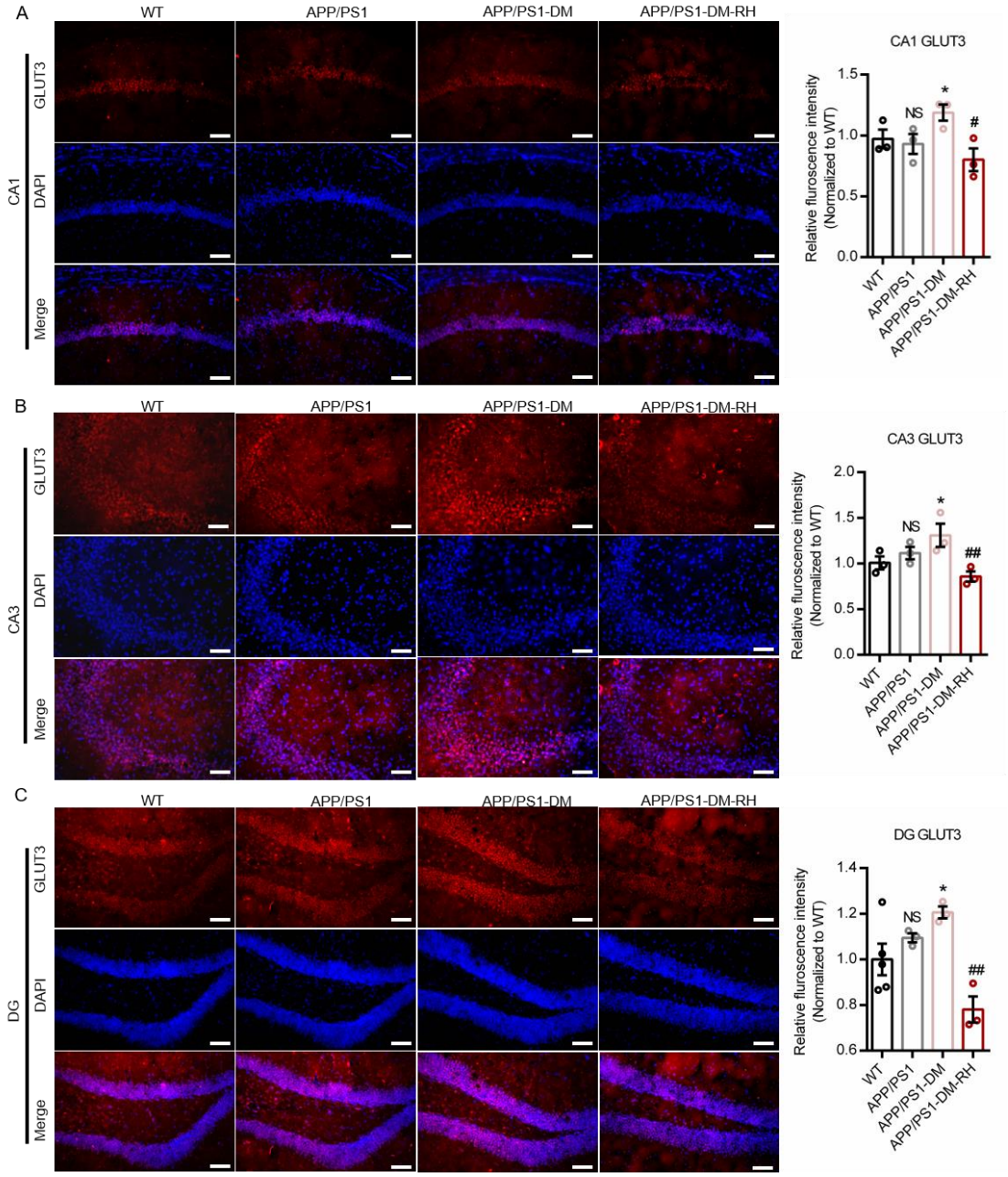

Figure S6, related to Figure 6. GLUT3 expression in hippocampus. (A-C) Representative images of GLUT3 (red) and DAPI (blue) immunostaining in hippocampal area of CA1 (A), CA3 (B) and DG (C) from WT, APP/PS1, APP/PS1-DM, and APP/PS1-DM-RH mice. Scale bar, 100μm. Quantitative results are showed in the right (n=3 mice for each group). The data are expressed as the mean ± SEM. Statistical significance was assessed using unpaired student's T test *$P<0.05$, APP/PS1-DM VS APP/PS1; $^{\#}P<0.05$, $^{\#\#}P<0.01$ and $^{\#\#\#}P<0.001$, APP/PS1-DM VS APP/PS1-DM-RH; WT VS APP/PS1, no significant difference (NS).

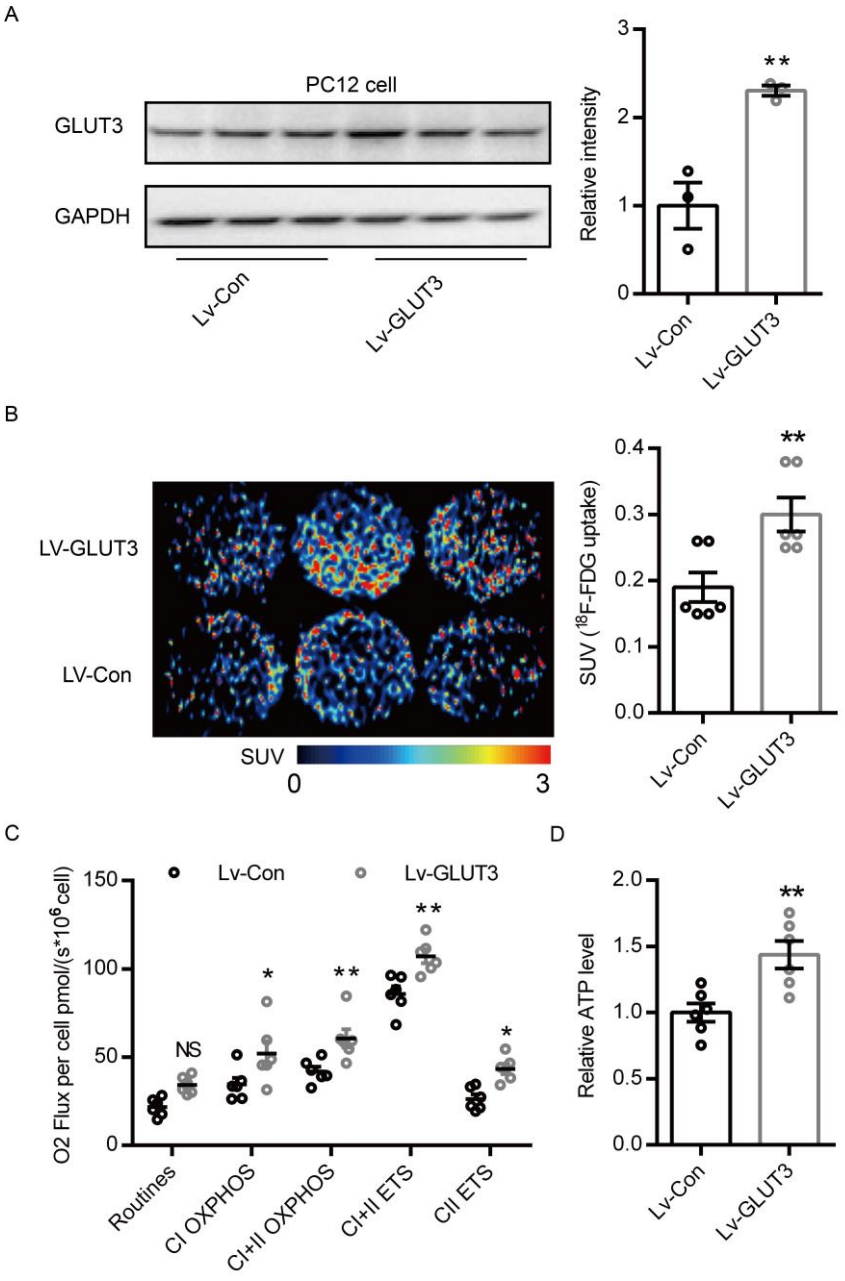

Figure S7, Related to Figure 6. GLUT3 over-expression in PC12 improves mitochondrial function in PC12 cells. (A) Western blotting to assess GLUT3 overexpression in PC12 cells. Lv-Con, PC12 cells infected with empty recombinant lentiviral vector; Lv-GLUT3, PC12 cells infected with GLUT3 recombinant lentiviral vector. (**B)** Representative image and quantitative results show the ^{18}F-FDG uptake in PC12 cells with or without GLUT3 overexpression (n=6 for each group). **(C)** High-resolution respirometry measured the oxygen consumption capacity of mitochondria in PC12 cells (n=6 for each group). **(D)** ATP content in PC12 cells (n=6 for each group). The data are expressed as the mean ± SEM. Statistical significance was assessed using unpaired student's t test (panel A,B and D) or two-way ANOVA followed by Sidak's multiple comparisons test (panel C). *P＜0.05, **P＜0.01.

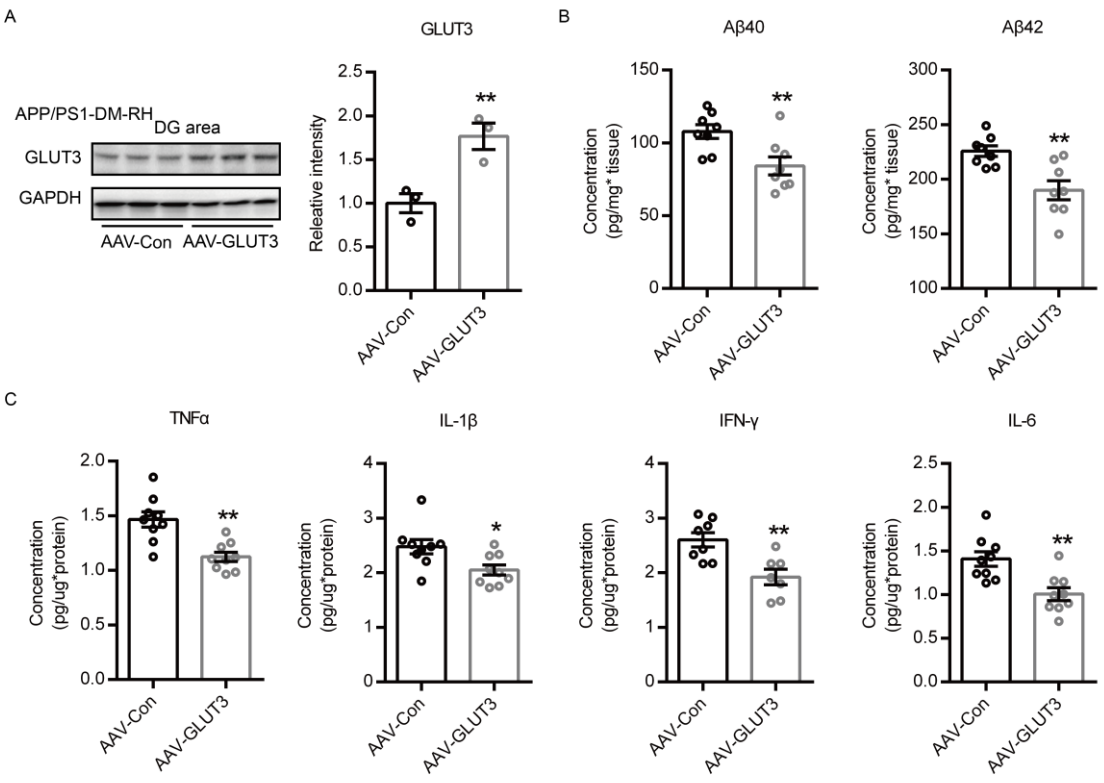

Figure S8, Related to Figure 6. GLUT3 over-expression in DG area of hippocampus improve RH induced AD-type pathologies in APP/PS1-DM-mice. (A) Western blot to assess GLUT3 abundance in DG area of hippocampus and the quantitative data shown in the right (n=3 mice for each group). AAV-Con, APP/PS1-DM-RH mice injected with empty adeno-associated virus in DG area; AAV-GLUT3, APP/PS1-DM-RH mice injected with adeno-associated virus expressing GLUT3 protein in DG area. (**B)** ELSIA to detect Aβ40 and Aβ42 in DG area of hippocampus (n=8 mice for each group). **(C)** Quantification of IL-6, IL-1β, IFN-γ and TNF-α by ELISA in DG area of hippocampus (n=9 mice for each group). The data are expressed as the mean ± SEM. Statistical significance was assessed using unpaired student's t test. **P*＜0.05, ***P*＜0.01.

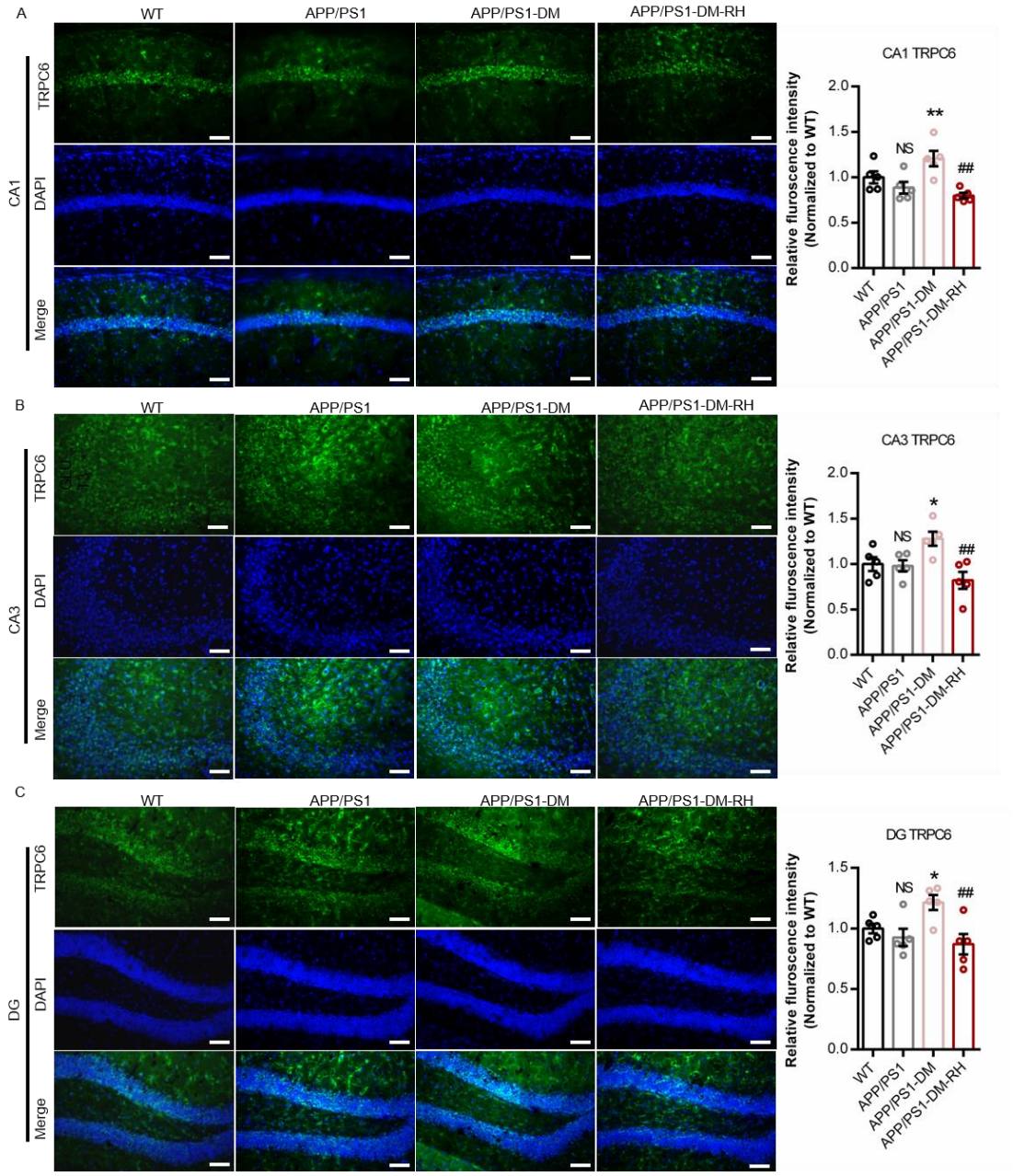

Figure S9, related to Figure 7. TRPC6 expression in hippocampus. (A-C) Representative images of TRPC6 (green) and DAPI (blue) immunostaining in hippocampal area of CA1 (A), CA3 (B) and DG (C) from WT, APP/PS1, APP/PS1-DM, and APP/PS1-DM-RH mice. *Scale bar*, 100μm. Quantitative results are showed in the right (n=5 mice for each group). The data are expressed as the mean ± SEM. Statistical significance was assessed using unpaired student's t test. $^{*}P<0.05$, APP/PS1-DM VS APP/PS1; $^{\#\#}P<0.01$, APP/PS1-DM VS APP/PS1-DM-RH; WT VS APP/PS1, no significant difference (NS).

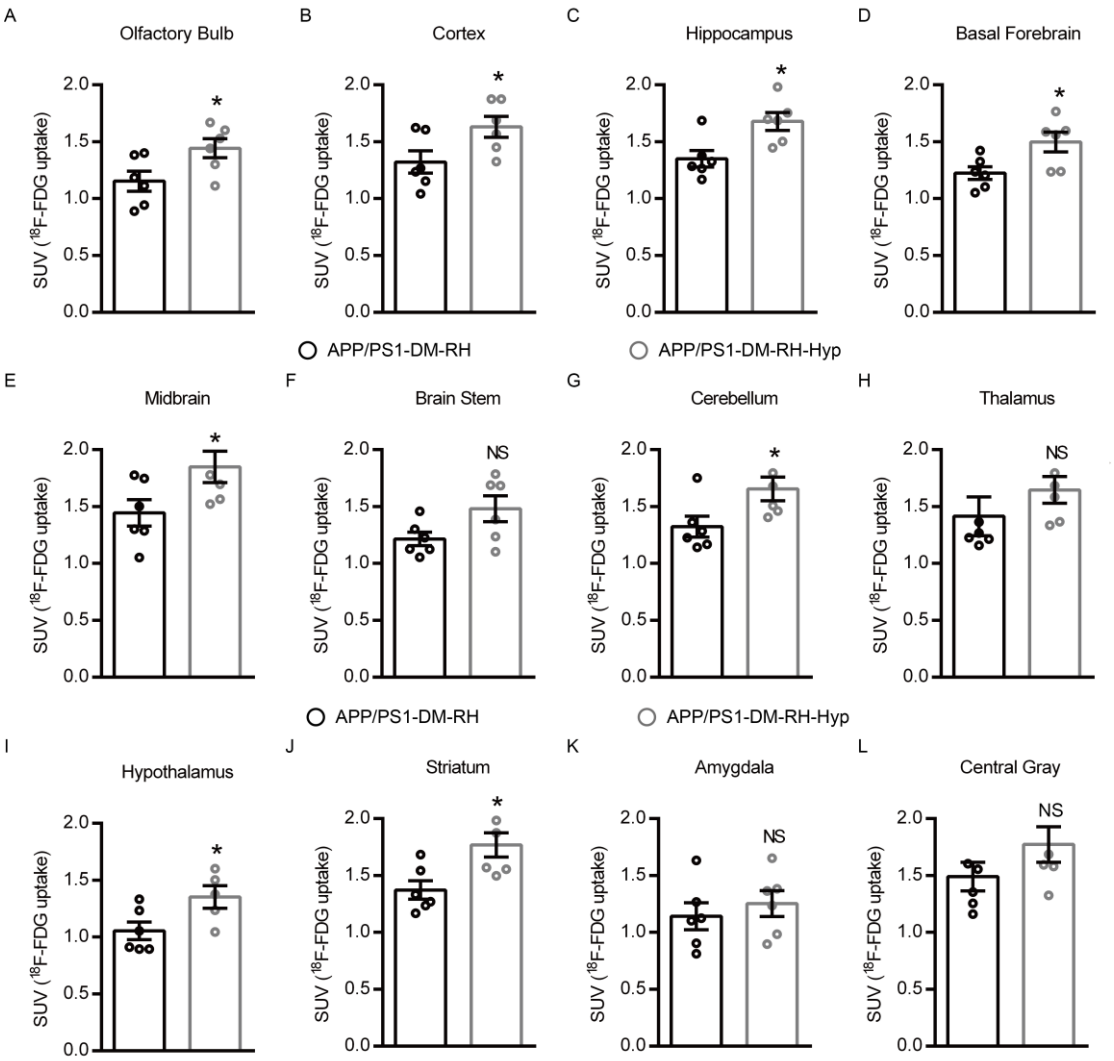

Figure S10, Related to Figure 7. Whole brain ^{18}F-FDG uptake. (A-L) The standard uptake value (SUV) of ^{18}F-FDG in different brain regions measured by ^{18}F-FDG PET/CT scanning (n=6 mice for each group). The data are expressed as the mean ± SEM. Statistical significance was assessed using unpaired student's t test. $^{*}P<0.05$ and $^{**}P<0.01$; NS, no significant difference.

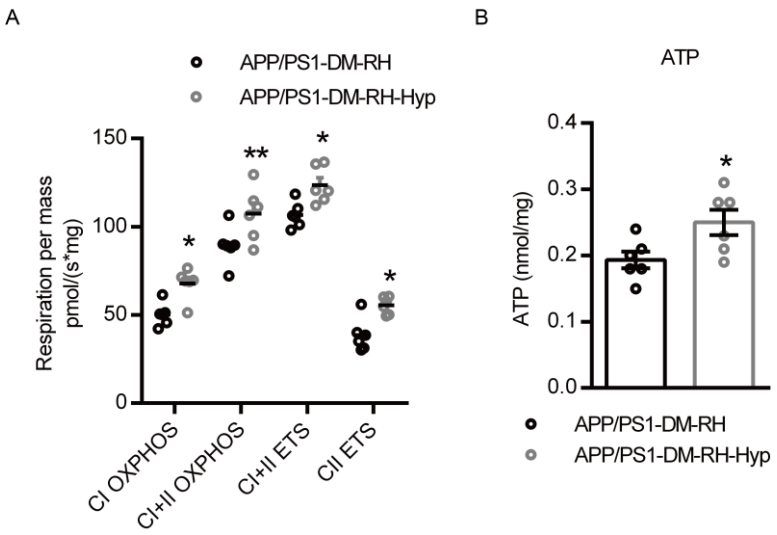

Figure S11, Related to Figure 7. Hyperforin treatment improves mitochondrial function. (A) High-resolution respirometry measured the oxygen consumption capacity of hippocampal mitochondria (n=6 for each group). **(B)** ATP content in hippocampus (n=6 for each group). The data are expressed as the mean ± SEM. Statistical significance was assessed using unpaired student's t test (panel B) or two-way ANOVA followed by Sidak's multiple comparisons test (panel A). *$P<$ 0.05, **$P<0.01$.

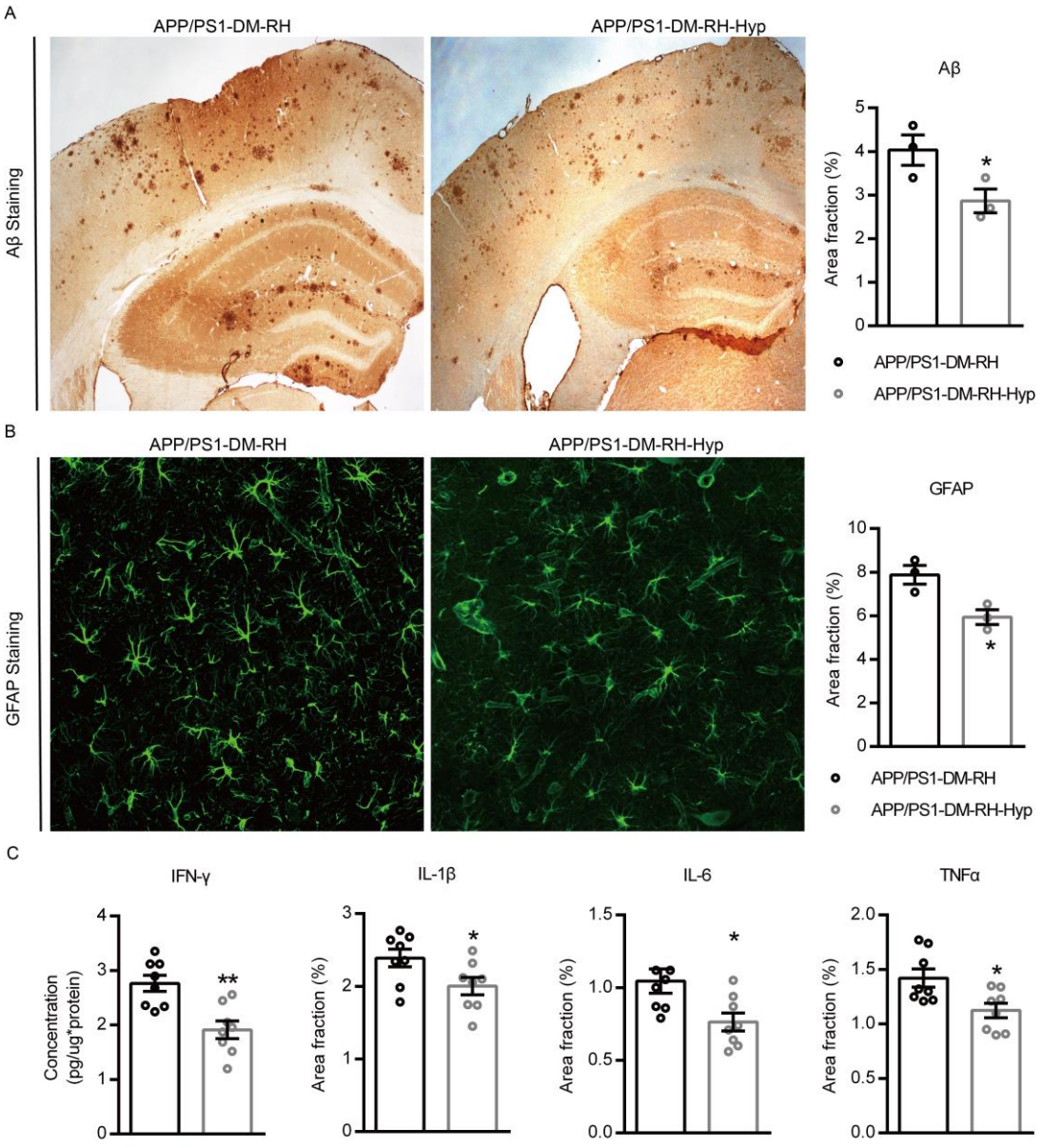

Figure S12, Related to Figure 7. Hyperforin treatment improves AD-type pathologies. (A) Representative images of Aβ immunohistochemistry staining (n=3 mice for each group). Hyp, hyperforin. **(B)** Representative images of GFAP immunofluorescent staining (n=3 mice for each group). **(C)** Quantification of IFN-γ、IL-1β、IL-6 and TNFα by ELISA in hippocampal homogenates (n=8 mice for each group). The data are expressed as the mean ± SEM. Statistical significance was assessed using unpaired student's t test. **P*＜0.05 and ***P*＜0.01; NS, no significant difference.

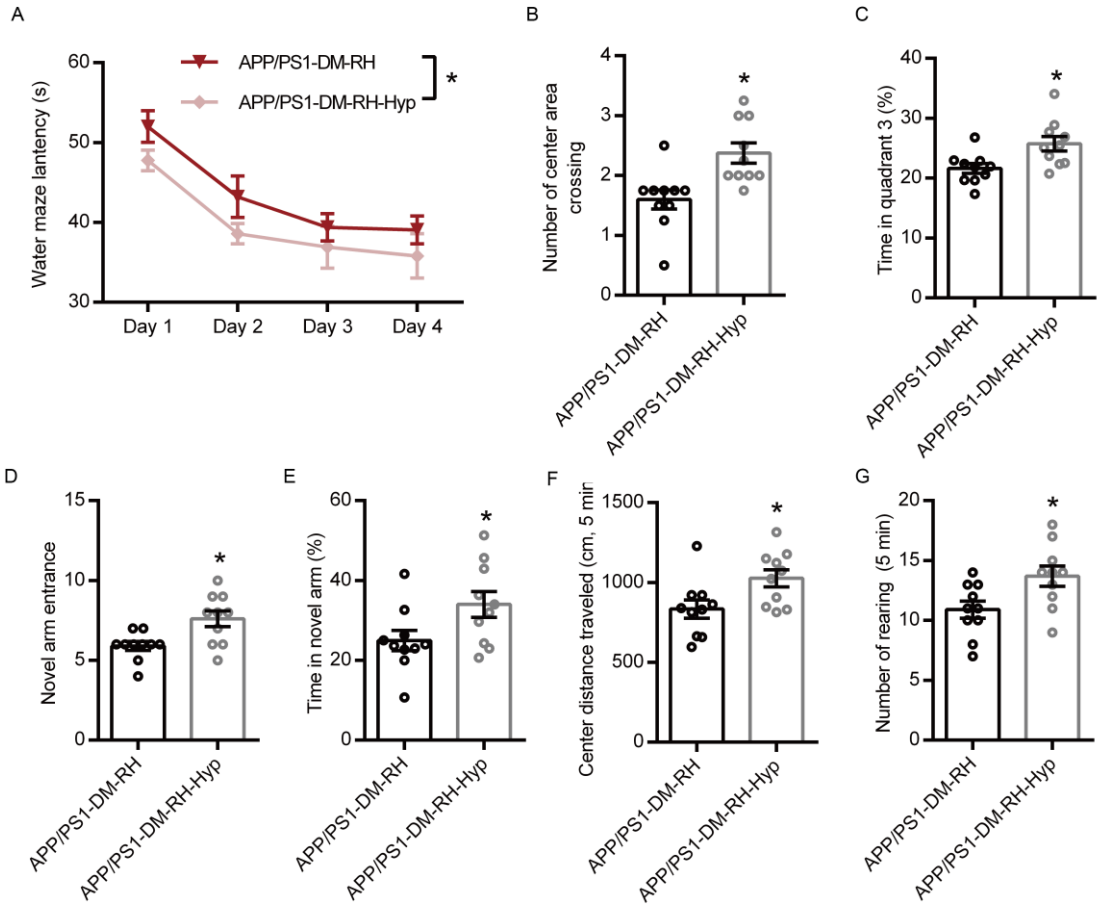

Figure S13, Related to Figure 7. The performances of mice treated with hyperforin in behavioral tests. (A-C) Escape latency during platform trials (A), number of center area crossing (B) and time spend in quadrant 3 o (Q3, C) in probe test. **(D and E)** Novel arm entrance (D) and time spend in the novel arm (E) in Y-maze test. **(F-G)** Distance traveled in center region (F) and number of rearing (G). Hyp, hyperforin, a TRPC6 agonist. n=10 mice for each group. The data are expressed as the mean ± SEM. Statistical significances were assessed using two-way ANOVA followed (panel A) or unpaired student's t test (panel B-G). $^{*}P<0.05$.

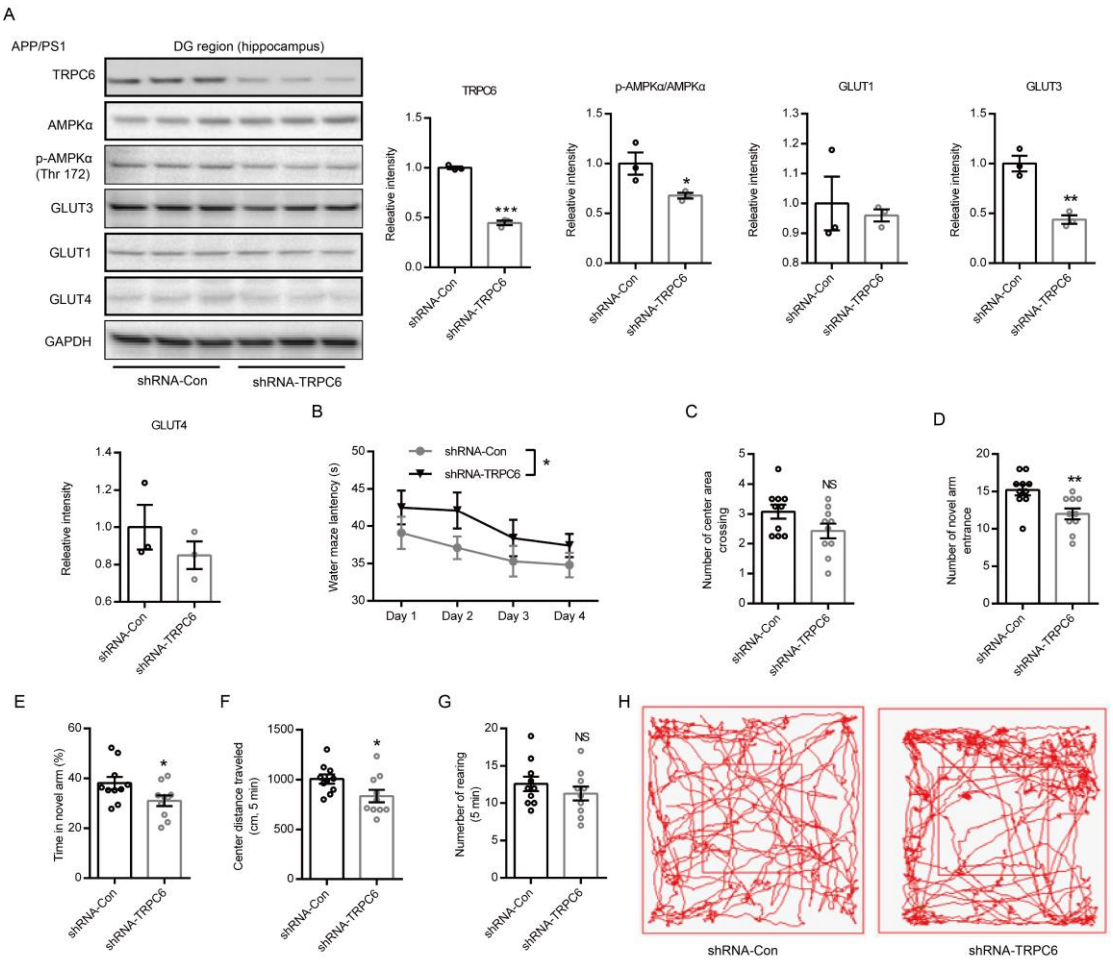

Figure S14, Related to Figure 7. TRPC6 down-regulation with shRNA. (A) Western-blot show the expression of TRPC6, AMPKα，p-AMPKα (Thr172)，GLUT3，GLUT1 and GLUT4 in DG hippocampal region. Quantitative data are shown on the right (n=3). shRNA-Con, APP/PS1 mice were bilaterally injected with empty AAV2/9 virus into DG area of hippocampus; shRNA-TRPC6, APP/PS1 mice were bilaterally injected with AAV2/9 virus expressing mouse shRNA (TRPC6) into DG area of hippocampus. **(B and C)** Escape latency during platform trials (B), number of center area crossing (C) in Morris water-maze test. **(D and E)** Number of novel arm entrance (D) and time spend in the novel arm (E) in Y-maze test. **(F-H)** Distance traveled in center region (F), number of rearing (G) and representative tracing graphs in open field test. n=10 mice for each group. The data are expressed as the mean ± SEM. Statistical significances were assessed using two-way ANOVA followed (panel B) or unpaired student's t test (panel A, C-G). $^{*}P<0.05$, $^{**}P<0.01$.

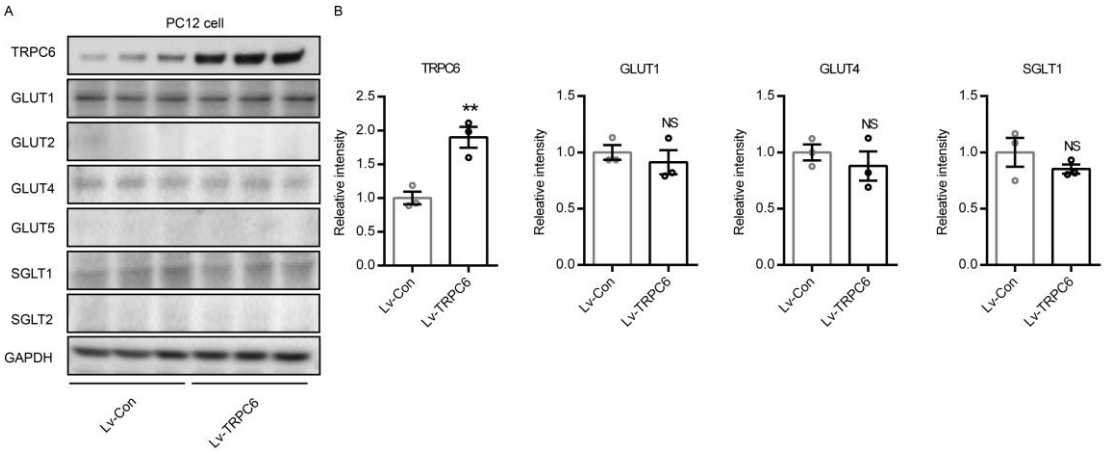

Figure S15, Related to Figure 7. GLUTs and SGLT1/2 expression. (A and B) Western blot and quantitation for TRPC6, GLUT1, GLUT2, GLUT4, GLUT5, SGLT1 and SGLT2 expression in PC12 cells. Lv-Con, the recombinant lentiviral vector; Lv-TRPC6, the recombinant lentiviral vector with TRPC6 over-expression. The data are expressed as the mean ± SEM. Statistical significance was assessed using unpaired student's t test. *$P<0.05$; NS, no significant difference.